

UNCLASSIFIED

AD 407 722

DEFENSE DOCUMENTATION CENTER

FOR

SCIENTIFIC AND TECHNICAL INFORMATION

CAMERON STATION, ALEXANDRIA, VIRGINIA



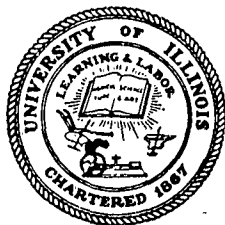
UNCLASSIFIED

NOTICE: When government or other drawings, specifications or other data are used for any purpose other than in connection with a definitely related government procurement operation, the U. S. Government thereby incurs no responsibility, nor any obligation whatsoever; and the fact that the Government may have formulated, furnished, or in any way supplied the said drawings, specifications, or other data is not to be regarded by implication or otherwise as in any manner licensing the holder or any other person or corporation, or conveying any rights or permission to manufacture, use or sell any patented invention that may in any way be related thereto.

407 722 CATALOGED BY DDC

AS AD No.

407 722



10

63-4-2

T.&A.M. REPORT NO. 248

APPLICATION OF FRACTURE MECHANICS TO ORTHOTROPIC PLATES

by

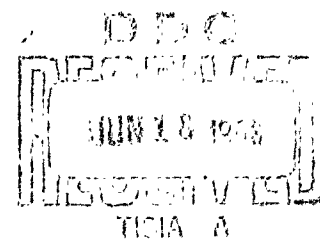
Edward M. Wu

Sponsored by

U. S. Naval Research Laboratory

Contract NO. Nonr 2947 (02) (x)

NRL Project 62 R05 19A



DEPARTMENT OF THEORETICAL AND APPLIED MECHANICS
UNIVERSITY OF ILLINOIS

T. & A. M. DEPARTMENT REPORTS:

The Department of Theoretical and Applied Mechanics at the University of Illinois, established in 1890 as a separate unit of the College of Engineering, has the following threefold purpose: (1) to offer instruction in engineering mechanics to undergraduate students, (2) to teach and train graduate students in the field of mechanics, and (3) to conduct a comprehensive research program resulting in the extension of knowledge in all branches of mechanics and related fields. From its inception, the department has offered courses in mechanics in partial fulfillment of the degree requirements of the other departments of the College and, since 1957, the degree of *Bachelor of Science* in Engineering Mechanics has been administered by the department. The granting of graduate degrees originated in 1908, both *Master of Science* and *Doctor of Philosophy* degrees being offered. Research is considered to be a basic part of the educational program; strong emphasis is placed on the fact that the functions of teaching and research go hand in hand for the most complete and effective development of both students and staff.

In general, the research studies are of a fundamental nature that supplement the regular educational functions of the department. They either show the application of the accepted concepts of the engineering sciences to problems in widely divergent fields or produce new concepts with which to attack specialized aspects of problems. Current projects are in the fields of mechanical properties of materials, mechanics of fluids, mechanics of solids, and dynamics. Many of these studies are of a complex analytical nature. However, extensive facilities and unique special equipment are also available for research and advanced study of engineering components which operate under extreme environmental conditions that lead to new problems for which standard design procedures are inadequate. Ten different laboratories are operated with special facilities for studies of concrete, fluid mechanics, fatigue, properties of metals, plastics, vibration, photoelasticity, creep, railroad rails and wheels, and experimental strain measurements employing electronic instrumentation.

The results of research studies conducted in the department are generally disseminated in *T. & A. M. Department Reports*. These present information of an enduring nature, such as the final report of a research contract, and in turn are given a wide initial distribution. After the remainder of the initial printing has been requested and distributed, copies are available on loan (or on purchase in microfilm form)* from the Acquisitions Department of the Library, University of Illinois, Urbana, Illinois. A list of recent reports is included inside the back cover of this report.

*For further information
address inquiries to:*

T. J. Dolan, Head of the Department
212 Talbot Laboratory
Urbana, Illinois

* Charges for microfilm copy are 4¢ per exposure plus mailing cost and 25¢ service charge.

Technical Memo No.

T&AM Report No. 248

APPLICATION OF FRACTURE MECHANICS
TO ORTHOTROPIC PLATES

by

Edward M. Wu

Sponsored by

U. S. Naval Research Laboratory

Contract No. Nonr 2947 (02)(x)

NRL Project 62 R05 19 A

Department of Theoretical and Applied Mechanics

University of Illinois

Urbana, Illinois

June, 1963

ACKNOWLEDGMENT

This investigation was part of the work in the study of fracture mechanics of fiber glass reinforced plastics supported by the Naval Research Laboratory through the Polaris Contract under the direction of Professor H. T. Corten. This investigation was conducted at the University of Illinois in the Department of Theoretical and Applied Mechanics of which Professor T. J. Dolan is Head.

Special acknowledgment is due to Professor H. T. Corten for his helpful criticism and suggestions.

Acknowledgment is also due to the personnel in the Fracture Research Laboratory in the Department of Theoretical and Applied Mechanics who offered simulating discussions and assistance in the various phases of this program. The author is indebted to R. C. Reuter for rendering valuable assistance in carrying out the experiments and G. Mercer for constructing the experimental apparatus and Mrs. H. Corray for preparing the manuscript.

ABSTRACT

The Griffith-Irwin (or linear-elastic) fracture concept was used to investigate the feasibility of the application of fracture mechanics to orthotropic plates. The problem of an infinite plate containing a single crack orientated in the direction of one of the planes of elastic symmetry of the plate subjected to arbitrary plane loading was examined. Two analytical crack tip stress analyses for this case were presented, and unlike the isotropic case, the stress distributions were observed to be dependent on the material constants. However, as in the isotropic case the crack tip stress singularity was observed to be $r^{-1/2}$ and stress intensity factors $k_1 = \sigma\sqrt{a}$ and $k_2 = \tau\sqrt{a}$ for loading symmetric and skew-symmetrical to the crack respectively could be used. Further, the existence of a functional relation between k_1 and k_2 was proposed.

Results of the experimental investigation using balsa wood plates indicated that the critical stress intensity factors k_{1c} and k_{2c} were constants for tension and pure shear. Moreover, under combined tension and shear, k_{1c} and k_{2c} were found to be related by the function $\left(\frac{k_1}{k_{1c}}\right)^2 + \left(\frac{k_2}{k_{2c}}\right)^2 = 1$ which satisfied the physical considerations.

TABLE OF CONTENTS

	Page
I. PRELIMINARY REMARKS	1
II. ANALYSIS	2
A. Introduction to Analysis	2
B. Analysis	3
1. Solution by Westergaard Type of Stress Function	5
a) Case 1: Symmetric Loading	7
b) Case 2: Skew-Symmetric Loading	10
2. Solution by Lekhnitskii's Method	13
3. Comparison of the Two Solutions	16
C. Comparison of the Crack Tip Stress Distribution in an Orthotropic Plate to that in an Isotropic Plate	18
III. EXPERIMENTAL PROGRAM	20
A. Introduction to the Experimental Investigation	20
1. Purpose of the Experimental Program	20
2. Experimental Set-up	20
B. Testing Procedure	21
1. Tension Tests	22
2. Combined Tension and Shear and Pure Shear Tests	22
C. Interpretation of Data and Results	23
D. Discussion of Results	24
E. Discussion of Experimental Accuracy	28
IV. SUMMARY AND RECOMMENDATIONS FOR FURTHER INVESTIGATION	32
V. REFERENCES	33

I. PRELIMINARY REMARKS

In many engineering applications, flaws and minute cracks are observed to extend, leading to fracture at nominal stress levels below that of the yield strength of the structures. The study of the mechanics of fracture and attempts to predict the combination of crack length and stress which would lead to failure by spontaneous crack extension have been undertaken by many investigators. Fracture mechanics thus developed in the past 20 years has achieved remarkable success in applications to isotropic materials. Since many engineering materials are anisotropic, it is logical to analyze the parameters involved and examine whether fracture mechanics can be applied to anisotropic materials as well.

A special but important group of anisotropic materials, the orthotropic material, was chosen for analysis. This investigation is applicable to single as well as composite materials of two or more components which are grossly homogeneous, but which possess orthotropic properties. Some important examples are wood, oriented glass fiber reinforced plastics and high strength wire reinforced metals and plastics.

The investigation consists of two parts. In the first part, a theoretical analysis of the stress distribution in the vicinity of the tip of a crack in an orthotropic plate is presented. In the second part, an experimental program is designed to verify the analytical findings. This study of orthotropic materials was undertaken in an attempt to shed light upon the application of fracture mechanics to general composite materials made of metals as well as non-metals.

II. ANALYSIS

A. Introduction to Analysis

The quasi-static stability criterion of a crack in a linear isotropic material was formulated by Griffith [1] * and later extended by Irwin [2]. In its simplest form the linear-elastic (or Griffith-Irwin) fracture theory states that the critical energy dissipation rate per unit area associated with an unstable crack extension is a constant for a given material. In the formulation of this theory, the following assumptions are made: 1) the material is macroscopically isotropic and homogeneous, 2) the material is ideally elastic, 3) infinitesimal linear elasticity is applicable for stress analysis in the vicinity of the tip of the crack. Irwin, upon defining three kinematically possible modes of crack extension, was able to compute the strain energy release rates, \mathcal{G}_1 , \mathcal{G}_2 and \mathcal{G}_3 , associated with each mode.

Further, in examining the elastic stress analysis, it was observed that the stress intensity factors k_1, k_2 and k_3 for each of the three modes are directly related to the respective strain energy release rates $\mathcal{G}_1, \mathcal{G}_2$ and \mathcal{G}_3 . Consequently, the magnitude of the critical stress intensity factors was also associated with unstable crack propagation. Based on the linear-elastic fracture theory, many problems in brittle fracture of isotropic materials have been described with a useful degree of engineering accuracy when similitude was maintained between the model and the actual crack extension problems.

Obviously, the Griffith-Irwin fracture concept is not limited to isotropic materials. In order to gain insight to the feasibility of application of fracture mechanics to anisotropic materials, the simplest case of anisotropy - the orthotropic material - is considered.

A material is said to be orthotropic when it possesses three orthogonal planes of elastic symmetry. The majority of the orthotropic engineering materials, such as plywood and some fiberglass reinforced plastics, possess such properties. However, if the analysis is limited to materials which possess only two orthogonal planes of elastic symmetry, the complexity of the mathematical formulation of their constitutive equations is considerably reduced. Limiting the analysis to such a material corresponds to the study of only one layer of the plywood, or only one layer of the reinforced plastic with glass fibers orientated all in one direction. Nevertheless, in order that the fracture mechanics aspects of the problem shall not be subdued by the algebraic complexity of the

* Numbers in brackets designate References listed.

more general problem, the use of a simplified model has to be tolerated.

An orthotropic plate which possesses two elastic symmetries containing a single crack subjected to arbitrary plane tractions with bending absent, as shown in Fig. 1b, will be considered. The imposed conditions are:

- 1) the material is linearly elastic
- 2) the plate is thin and extends infinitely in all directions from a crack
- 3) the crack is straight and "sharp" i. e., a straight line of discontinuity in the plate
- 4) the crack is parallel to one of the principle planes of elastic symmetry
- 5) the influence of environment is neglected

Although the above conditions are necessary for the mathematical analysis which follows they do not significantly restrict its applications. If a crack is small in the actual structure compared to its surrounding dimensions, a sufficient similitude exists between the mathematical model and the actual crack.

B. Analysis

When a body containing a crack is subjected to external tractions, the sole influence of the external conditions on the crack (the influence of environment is neglected) is the state of stress around the crack. If the crack is to extend, the state of stress or other parameters associated with the state of stress at the tips of the crack must reach a critical value for the given material of which the body is composed. Then, to analyze the crack stability in an orthotropic plate, an examination of the state of stress in the vicinity of the tips of the crack is in order.

For the plane problem of a linear elastically orthotropic material, the generalized Hooke's law may be written:

$$\begin{aligned}\epsilon_x &= a_{11} \sigma_x + a_{12} \sigma_y + a_{16} \tau_{xy}, \\ \epsilon_y &= a_{12} \sigma_x + a_{22} \sigma_y + a_{26} \tau_{xy}, \\ 2\epsilon_{xy} &= a_{16} \sigma_x + a_{26} \sigma_y + a_{66} \tau_{xy}.\end{aligned}\tag{1}$$

The compatibility equation for plane deformation is

$$\frac{\partial^2 \epsilon_x}{\partial y^2} + \frac{\partial^2 \epsilon_y}{\partial x^2} = 2 \frac{\partial^2 \epsilon_{xy}}{\partial x \partial y}.\tag{2}$$

In order to simplify the constitutive equations, the x and y axes can be oriented in such a way that they coincide with the principle planes of elastic symmetry. For this orientation of axes,

$$a_{16} = a_{26} = 0. \quad (3)$$

Substitution of Eqs. (2) and (3) into Eq. (1) gives

$$a_{11} \frac{\partial^2 \sigma_x}{\partial y^2} + a_{12} \left(\frac{\partial^2 \sigma_x}{\partial x^2} + \frac{\partial^2 \sigma_y}{\partial y^2} \right) + a_{22} \frac{\partial^2 \sigma_y}{\partial x^2} - a_{66} \frac{\partial^2 \tau_{xy}}{\partial x \partial y} = 0. \quad (4)$$

When body forces are neglected the equations of equilibrium and compatibility are satisfied by Airy's stress function U, and the stresses can be expressed as

$$\sigma_x = \frac{\partial^2 U}{\partial y^2}, \quad \sigma_y = \frac{\partial^2 U}{\partial x^2} \text{ and } \tau_{xy} = - \frac{\partial^2 U}{\partial x \partial y}. \quad (5)$$

Also, the material constants a_{ij} can be expressed in terms of the usual engineering notations, i. e.

$$a_{11} = \frac{1}{E_x}, \quad a_{22} = \frac{1}{E_y}, \quad a_{12} = - \frac{\nu_x}{E_x} = - \frac{\nu_y}{E_y} \text{ and } a_{66} = \frac{1}{G_{xy}}. \quad (6)$$

Using the relationships given by Eqs. (5) and (6), Eq. (4) becomes

$$\frac{\partial^4 U}{\partial x^4} + 2 \left(\frac{E_y}{2G_{xy}} - \nu_y \right) \frac{\partial^4 U}{\partial x^2 \partial y^2} + \left(\frac{E_y}{E_x} \right) \frac{\partial^4 U}{\partial y^4} = 0. \quad (7)$$

The problem therefore reduces to the solution of the above 4th order homogeneous partial differential equation whose auxiliary equation is

$$s^4 + 2 \left(\frac{E_y}{2G_{xy}} - \nu_y \right) s^2 + \left(\frac{E_y}{E_x} \right) = 0. \quad (8)$$

It can be shown that Eq. (8) has no real roots [3]. Further since the coefficients are real constants (the elastic constants are real), the roots must be in conjugate pairs, i. e., they are $s_1, s_2, \bar{s}_1, \bar{s}_2$. [4]

$$\begin{aligned} \text{If } s_1 &= (\alpha + i\beta), \\ \text{then } s_2 &= (-\alpha + i\beta), \\ \text{and } \bar{s}_1 &= (\alpha - i\beta), \\ \bar{s}_2 &= -(\alpha + i\beta). \end{aligned} \quad (9)$$

Substitution of Eqs. (9) into (8) gives

$$\begin{aligned} 2\beta^2 &= \left(\frac{E_x}{E_y}\right)^{1/2} + \left(\frac{E_x}{2G_{xy}} - \nu_x\right), \\ 2\alpha^2 &= \left(\frac{E_x}{E_y}\right)^{1/2} - \left(\frac{E_x}{2G_{xy}} - \nu_x\right). \end{aligned} \quad (10)$$

Then, the general solution of Eq. (6) is

$$U = Z_1(\xi_1) + Z_2(\bar{\xi}_1) + Z_3(\xi_2) + Z_4(\bar{\xi}_2) \quad (11)$$

where

$$\xi_1 = x + s_1 y, \quad \bar{\xi}_1 = x + \bar{s}_1 y, \quad \xi_2 = x + s_2 y \text{ and } \bar{\xi}_2 = x + \bar{s}_2 y.$$

In order to obtain the function U which satisfies the boundary conditions for the plate containing a crack, two solutions will be outlined. First, a technique employing a Westergaard type of stress function will be discussed. Following this a brief outline of a stress function type of procedure developed primarily by S. G. Lekhnitskii* will be given.

1. Solution by Westergaard Type of Stress Function:

From physical consideration, it is known that U must be real. Therefore Eq. (11) can be written in the following form:**

$$U = A \operatorname{Re} [Z_A(\xi_1)] + B \operatorname{Im} [Z_B(\xi_1)] + C \operatorname{Re} [Z_C(\xi_2)] + D \operatorname{Im} [Z_D(\xi_2)] \quad (12)$$

where

$$\begin{aligned} \xi_1 &= x + s_1 y = x + (\alpha + i\beta) y = x_1 + iy_1, \\ \xi_2 &= x + s_2 y = x + (-\alpha + i\beta) y = x_2 + iy_2. \end{aligned} \quad (13)$$

The arbitrary external tractions are treated in two separated parts. 1) Loading symmetric with respect to the crack and, 2) loading skew-symmetric with respect to the crack. The following notations are adopted:

The complex functions Z_i in Eq. (11) for symmetric loading are

$$Z_1(\xi_1) = Z_{11}, \quad Z_1(\xi_2) = Z_{12}.$$

* A third method of solution employing integral equations by D. D. Ang and M. L. Williams is also available [5].

** This can be seen by expanding the arbitrary functions Z_i from Eq. (11) in power series.

And for the skew-symmetric loading, they are

$$Z_2(\xi_1) = Z_{21}, \quad Z_2(\xi_2) = Z_{22}.$$

In general

$$Z_{ij} = Z_i(\xi_j).$$

The first subscript refers to the nature of the traction, "1" for symmetric, "2" for skew-symmetric. The second subscript "1" or "2" refers to the complex variable ξ_1 and ξ_2 respectively.

Westergaard [6] observed that the stress around a mathematical crack on the axis $y = 0$ can be solved by a single stress function in isotropic materials. Irwin [7] later pointed out that in specially orthotropic material ($a_{16} = a_{26} = 0$) the counterparts of a Westergaard type of stress functions are as follows*:

a) Symmetric loading

$$U_1 = \frac{1}{2} \operatorname{Re} [\bar{Z}_1(\xi_1) + \bar{Z}_1(\xi_2)] + \frac{\beta}{2\alpha} \operatorname{Im} [\bar{Z}_1(\xi_1) - \bar{Z}_1(\xi_2)], \quad \text{and} \quad (14)$$

b) Skew symmetric loading

$$U_2 = -\frac{1}{2\alpha} \operatorname{Re} [\bar{Z}_2(\xi_1) - \bar{Z}_2(\xi_2)], \quad (15)$$

where **

$$\frac{d\bar{Z}_{ij}}{d\xi_j} = \bar{Z}_{ij}, \quad \frac{d\bar{Z}_{ij}}{d\xi_j} = Z_{ij} \quad \text{and} \quad \frac{dZ_{ij}}{d\xi_j} = Z'_{ij} \quad \begin{array}{l} i = 1, 2 \\ j = 1, 2 \end{array} \quad (16)$$

and

$$Z_{ij} = Z_i(\xi_j)$$

From the Cauchy-Riemann relationships the following relations can be observed:

$$\begin{aligned} \operatorname{Re} \bar{Z}_{ij} &= \frac{\partial \operatorname{Re} \bar{Z}_{ij}}{\partial x_j} = \frac{\partial \operatorname{Im} \bar{Z}_{ij}}{\partial y_j}, & i = 1, 2 \\ & & j = 1, 2 \\ \operatorname{Im} \bar{Z}_{ij} &= \frac{\partial \operatorname{Im} \bar{Z}_{ij}}{\partial x_j} = -\frac{\partial \operatorname{Re} \bar{Z}_{ij}}{\partial y_j}. \end{aligned} \quad (17)$$

* Irwin was instrumental in adopting Westergaard-type of stress functions to orthotropic materials [7]. Hence the notation used by Westergaard and Irwin was adopted in this analysis.

** Note, the summation convention is not used here.

Upon noting that

$$\frac{\partial x}{\partial x_1} = 1, \quad \frac{\partial y}{\partial x_1} = 0; \quad \frac{\partial y}{\partial y_1} = \frac{1}{\beta}, \quad \frac{\partial x}{\partial y_1} = -\frac{\alpha}{\beta},$$

$$\frac{\partial x}{\partial x_2} = 1, \quad \frac{\partial y}{\partial x_2} = 0, \quad \frac{\partial y}{\partial y_2} = \frac{1}{\beta}, \quad \frac{\partial x}{\partial y_2} = \frac{\alpha}{\beta}.$$

and from Eq. (13) and using the rules of differentiation to operate on Eq. (17), the following relations are obtained;

$$\begin{aligned} \frac{\partial \operatorname{Re} \bar{Z}_{i1}}{\partial x} &= \operatorname{Re} Z_{i1}, \\ \frac{\partial \operatorname{Im} \bar{Z}_{i1}}{\partial x} &= \operatorname{Im} Z_{i1}, \end{aligned} \quad i = 1, 2 \quad (18)$$

$$\begin{aligned} \frac{\partial \operatorname{Re} \bar{Z}_{i1}}{\partial y} &= \alpha \operatorname{Re} \bar{Z}_{i1} - \beta \operatorname{Im} \bar{Z}_{i1}, \\ \frac{\partial \operatorname{Im} \bar{Z}_{i1}}{\partial y} &= \alpha \operatorname{Im} \bar{Z}_{i1} + \beta \operatorname{Re} \bar{Z}_{i1}, \end{aligned}$$

and

$$\begin{aligned} \frac{\partial \operatorname{Re} \bar{Z}_{i2}}{\partial x} &= \operatorname{Re} \bar{Z}_{i2}, \\ \frac{\partial \operatorname{Im} \bar{Z}_{i2}}{\partial x} &= \operatorname{Im} \bar{Z}_{i2}, \end{aligned} \quad i = 1, 2 \quad (19)$$

$$\begin{aligned} \frac{\partial \operatorname{Re} \bar{Z}_{i1}}{\partial y} &= -\alpha \operatorname{Re} \bar{Z}_{i2} - \beta \operatorname{Im} \bar{Z}_{i1}, \\ \frac{\partial \operatorname{Im} \bar{Z}_{i2}}{\partial y} &= -\alpha \operatorname{Im} \bar{Z}_{i2} + \beta \operatorname{Re} \bar{Z}_{i2}. \end{aligned}$$

With these equations, the stress distribution for the case where loading is symmetric to the crack and the case where loading is skew-symmetric to the crack can be computed.

a. Case 1: Symmetric Loading

Returning to Eq. (14) and adopting the notation which was described following Eq. (13), the Westergaard-Irwin stress function can be written as

$$U_1 = \frac{1}{2} \operatorname{Re} \bar{Z}_{11} + \bar{Z}_{12} + \frac{\beta}{2\alpha} \operatorname{Im} \bar{Z}_{11} - \bar{Z}_{12}. \quad (20)$$

Using the results of Eq. (18) and (19) for $i = 1$, substitution of Eq. (20) into Eq. (5) gives

$$\begin{aligned}\sigma_x &= \frac{\alpha^2 + \beta^2}{2} \operatorname{Re}(Z_{11} + Z_{12}) - \frac{\beta}{\alpha} \operatorname{Im}(Z_{11} - Z_{12}), \\ \sigma_y &= \frac{1}{2} \operatorname{Re}(Z_{11} + Z_{12}) + \frac{\beta}{2\alpha} \operatorname{Im}(Z_{11} - Z_{12}), \\ \tau_{xy} &= -\frac{\alpha^2 + \beta^2}{2\alpha} \operatorname{Re}(Z_{11} - Z_{12}).\end{aligned}\quad (21)$$

For an infinite plane containing a single crack extending from $x = a$ to $x = -a$, Westergaard [6] showed that the function $Z(\xi) = \frac{f(\xi)}{\sqrt{\xi^2 - a^2}}$ satisfied the boundary conditions and produced a branch cut on $-a \leq x \leq +a$. Since no consideration of the material properties of the plate entered into the choice of this function, it would be applicable to orthotropic as well as isotropic materials. Thus the complex functions Z_{1j} for the Eq. (21) is

$$Z_{1j} = \frac{f_1(\xi_j)}{\sqrt{\xi_j^2 - a^2}} \quad j = 1, 2 \quad (22)$$

For a crack with traction free surfaces, the boundary conditions are

$$\begin{aligned}\tau_{xy} &= 0, \\ \sigma_y &= 0,\end{aligned} \quad \text{for } x \leq a \text{ and } y = 0. \quad (23)$$

From Eq. (13), note that on $y = 0$

$$\xi_1 = \xi_2 = x.$$

And from Eq. (22)

$$Z_{11} = Z_{12} \quad \text{on } y = 0.$$

Therefore the first condition of Eq. (23) is automatically satisfied from Eq. (21):

$$\begin{aligned}\sigma_x \Big|_{y=0} &= (\alpha^2 + \beta^2) \operatorname{Re}(Z_{11}), \\ \sigma_y \Big|_{y=0} &= \operatorname{Re}(Z_{11}) = \operatorname{Re}(Z_{12}) = \operatorname{Re}(Z_{1j}).\end{aligned}$$

In order that the second condition of Eq. (23) be satisfied,

$$\sigma_y \Big|_{\substack{y=0 \\ |x| \leq a}} = \operatorname{Re}(Z_{1j}) = \operatorname{Re} \frac{f_1(\xi_j)}{i H(x)} \Big|_{\substack{y=0 \\ |x| \leq a}} = 0, \quad (24)$$

where $H(x)$ is real. Equation (24) demands that

$$\operatorname{Im} f_1(\xi_j) \Big|_{\substack{y=0 \\ |x| \leq a}} = 0. \quad j = 1, 2 \quad (25)$$

It should also be noted that $f_1(\xi_j)$ is prescribed by the external loads far away from the crack. For the case of a pure tensile traction σ applied at infinity,

$$f_1(\xi_j) = \sigma \xi_j. \quad (26)$$

It can be seen that the conditions specified by Eq. (25) are satisfied by Eq. (26). Substitution of Eq. (26) and (22) into Eq. (21) gives the stress distribution at any point in the plate.

However, if examination of the stress intensity is limited to the neighborhood of the tips of the crack, certain simplification is possible. Due to symmetry, only the stress intensity around one crack tip need be examined.

For the stress near the vicinity of the tip of the crack, the location of the geometrical points around the tip of the crack can be expressed as $a + re^{i\theta}$ where $0 \leq |\theta| \leq \pi$. Recall from Eq. (13) that

$$\begin{aligned} \xi_1 &= x + s_1 y, \\ \xi_2 &= x + s_2 y. \end{aligned}$$

ξ_1, ξ_2 can be considered as complex variables of two non-orthogonal coordinates with non-normalized base vectors s_1 and s_2 . They can be defined in the following manner:*

$$\begin{aligned} \xi_1 &= x + s_1 y = a + r (\cos \theta + s_1 \sin \theta), \\ \xi_2 &= x + s_2 y = a + r (\cos \theta + s_2 \sin \theta). \end{aligned} \quad (27)$$

* Note that ξ_1 and ξ_2 are not the geometrical points at which the state of stress is under consideration. On the other hand, in the special case of isotropy, $\alpha = 0$ and $\beta = 1$ lead to $s_1 = s_2 = i$, or $\xi = a + r(\cos \theta + i \sin \theta) = a + re^{i\theta}$, i. e. ξ and the geometrical points coincide.

For the points in the vicinity of the tip of the crack,

$$r \ll a. \quad (28)$$

Eq. (28) implies that

$$f_1(k_j) \cong f_1(a) \quad (29)$$

Substitution of Eqs. (27) and (29) into Eq. (22) leads to

$$Z_{1j} \cong \frac{\sigma\sqrt{a}}{\sqrt{2r}(\cos\theta + s_j \sin\theta)} \quad j = 1, 2 \quad (30)$$

In the sequel, the approximation notation is dropped for convenience but it should be kept in mind that the expressions are applicable only in the vicinity of the crack tip.

Substitution of Eq. (30) into Eq. (21) gives the stress distribution around the tip of a crack in an infinite plane under tensile traction applied at infinity (Fig. 2a) as:

$$\begin{aligned} \sigma_x &= \frac{\sigma\sqrt{a}}{\sqrt{2r}} \frac{(\alpha^2 + \beta^2)}{2} \left[\operatorname{Re} \left(\frac{1}{\sqrt{\cos\theta + s_1 \sin\theta}} + \frac{1}{\sqrt{\cos\theta + s_2 \sin\theta}} \right) \right. \\ &\quad \left. - \frac{\beta}{\alpha} \operatorname{Im} \left(\frac{1}{\sqrt{\cos\theta + s_1 \sin\theta}} - \frac{1}{\sqrt{\cos\theta + s_2 \sin\theta}} \right) \right] \\ \sigma_y &= \frac{\sigma\sqrt{a}}{\sqrt{2r}} \frac{1}{2} \left[\operatorname{Re} \left(\frac{1}{\sqrt{\cos\theta + s_1 \sin\theta}} + \frac{1}{\sqrt{\cos\theta + s_2 \sin\theta}} \right) \right. \\ &\quad \left. + \frac{\beta}{\alpha} \operatorname{Im} \left(\frac{1}{\sqrt{\cos\theta + s_1 \sin\theta}} - \frac{1}{\sqrt{\cos\theta + s_2 \sin\theta}} \right) \right] \\ \tau_{xy} &= -\frac{\sigma\sqrt{a}}{\sqrt{2r}} \frac{(\alpha^2 + \beta^2)}{2\alpha} \left[\operatorname{Re} \left(\frac{1}{\sqrt{\cos\theta + s_1 \sin\theta}} - \frac{1}{\sqrt{\cos\theta + s_2 \sin\theta}} \right) \right] \end{aligned} \quad (31)$$

b. Case 2: Skew-Symmetric Loading

For external loading skew-symmetric to the crack, the Westergaard-Irwin stress function can be written as *

$$U_2 = -\frac{1}{2\alpha} \operatorname{Re} [Z_{21} - Z_{22}] \quad (32)$$

* Rewriting Eq. (15) using the notation described following Eq. 13.

Substitution of Eq. (32) into Eq. (5), using Eq. (18) and (19) for $i = 2$ yields

$$\begin{aligned}\sigma_x &= -\frac{1}{2\alpha} \left[(\alpha^2 - \beta^2) \operatorname{Re} (Z_{21} - Z_{22}) - 2\alpha\beta \operatorname{Im} (Z_{21} + Z_{22}) \right], \\ \sigma_y &= -\frac{1}{2\alpha} \operatorname{Re} (Z_{21} - Z_{22}), \\ \tau_{xy} &= \frac{1}{2\alpha} \left[\alpha \operatorname{Re} (Z_{21} + Z_{22}) - \beta \operatorname{Im} (Z_{21} - Z_{22}) \right].\end{aligned}\quad (33)$$

For a single crack, the complex functions Z_{2j} are

$$Z_{2j} = \frac{f_2(\xi_j)}{\sqrt{\xi_j^2 - a^2}}, \quad j = 1, 2 \quad (34)$$

The boundary conditions are

$$\begin{aligned}\sigma_y &= 0, \\ \tau_{xy} &= 0,\end{aligned}\quad \text{for } |x| \leq a \text{ and } y = 0. \quad (35)$$

Considerations similar to those in the symmetric case can be used. Equation (34) automatically satisfies the first condition of Eq. (35), and for the second condition to hold

$$\operatorname{Im} f_2(\xi_j) \Big|_{\substack{y=0 \\ |x| \leq a}} = 0 \quad j = 1, 2 \quad (36)$$

For a plate subjected to pure shearing traction at infinity

$$f_2(\xi_j) = \tau \xi_j. \quad (37)$$

Thus the approximate expressions for the complex functions defined by Eq. (34) in the vicinity of the crack tip are

$$Z_{2j} = \frac{\tau \sqrt{a}}{\sqrt{2r} \sqrt{\cos \theta + s_j \sin \theta}}, \quad j = 1, 2 \quad (38)$$

Substitution of Eq. (38) into Eq. (33) gives the stress distribution around the tip of a crack in an infinite plane under shearing traction at infinity (Fig. 2b) as:

$$\begin{aligned}
 \sigma_x &= \frac{\tau\sqrt{a}}{\sqrt{2r}} \left[-\frac{(\alpha^2 - \beta^2)}{2\alpha} \operatorname{Re} \left(\frac{1}{\sqrt{\cos \theta + s_1 \sin \theta}} - \frac{1}{\sqrt{\cos \theta + s_2 \sin \theta}} \right) \right. \\
 &\quad \left. + \beta \operatorname{Im} \left(\frac{1}{\sqrt{\cos \theta + s_1 \sin \theta}} + \frac{1}{\sqrt{\cos \theta + s_2 \sin \theta}} \right) \right], \\
 \sigma_y &= -\frac{\tau\sqrt{2}}{\sqrt{2r}} \frac{1}{2\alpha} \left[\operatorname{Re} \left(\frac{1}{\sqrt{\cos \theta + s_1 \sin \theta}} - \frac{1}{\sqrt{\cos \theta + s_2 \sin \theta}} \right) \right], \\
 \tau_{xy} &= \frac{\tau\sqrt{a}}{\sqrt{2r}} \left[\frac{1}{2} \operatorname{Re} \left(\frac{1}{\sqrt{\cos \theta + s_1 \sin \theta}} + \frac{1}{\sqrt{\cos \theta + s_2 \sin \theta}} \right) \right. \\
 &\quad \left. - \frac{\beta}{2\alpha} \operatorname{Im} \left(\frac{1}{\sqrt{\cos \theta + s_1 \sin \theta}} - \frac{1}{\sqrt{\cos \theta + s_2 \sin \theta}} \right) \right].
 \end{aligned} \tag{39}$$

Since Eq. (31) and (39) describe the stress distribution around the tip of the crack in plates of identical geometry (in each case, a single crack is present), the two solutions can be superimposed to describe any arbitrary plane traction. Then for the loading condition as shown in Fig. 2c, the crack tip stress distribution obtained by the Westergaard-Irwin method is

$$\begin{aligned}
 \sigma_x &= \frac{\sigma\sqrt{a}}{\sqrt{2r}} \frac{(\alpha^2 + \beta^2)}{2\alpha} \left[\alpha \operatorname{Re} \left(\frac{1}{\sqrt{\cos \theta + s_1 \sin \theta}} + \frac{1}{\sqrt{\cos \theta + s_2 \sin \theta}} \right) - \beta \operatorname{Im} \left(\frac{1}{\sqrt{\cos \theta + s_1 \sin \theta}} + \frac{1}{\sqrt{\cos \theta + s_2 \sin \theta}} \right) \right] \\
 &\quad - \frac{\tau\sqrt{a}}{\sqrt{2r}} \frac{1}{2\alpha} \left[(\alpha^2 - \beta^2) \operatorname{Re} \left(\frac{1}{\sqrt{\cos \theta + s_1 \sin \theta}} - \frac{1}{\sqrt{\cos \theta + s_2 \sin \theta}} \right) - 2\alpha\beta \operatorname{Im} \left(\frac{1}{\sqrt{\cos \theta + s_1 \sin \theta}} + \frac{1}{\sqrt{\cos \theta + s_2 \sin \theta}} \right) \right] \\
 \sigma_y &= \frac{\sigma\sqrt{a}}{\sqrt{2r}} \frac{1}{2\alpha} \left[\alpha \operatorname{Re} \left(\frac{1}{\sqrt{\cos \theta + s_1 \sin \theta}} + \frac{1}{\sqrt{\cos \theta + s_2 \sin \theta}} \right) + \beta \operatorname{Im} \left(\frac{1}{\sqrt{\cos \theta + s_1 \sin \theta}} - \frac{1}{\sqrt{\cos \theta + s_2 \sin \theta}} \right) \right] \\
 &\quad - \frac{\tau\sqrt{a}}{\sqrt{2r}} \frac{1}{2\alpha} \left[\operatorname{Re} \left(\frac{1}{\sqrt{\cos \theta + s_1 \sin \theta}} - \frac{1}{\sqrt{\cos \theta + s_2 \sin \theta}} \right) \right] \\
 \tau_{xy} &= \frac{\sigma\sqrt{a}}{\sqrt{2r}} \frac{(\alpha^2 + \beta^2)}{2\alpha} \left[\operatorname{Re} \left(\frac{1}{\sqrt{\cos \theta + s_1 \sin \theta}} - \frac{1}{\sqrt{\cos \theta + s_2 \sin \theta}} \right) \right] \\
 &\quad + \frac{\tau\sqrt{a}}{\sqrt{2r}} \frac{1}{2\alpha} \left[\alpha \operatorname{Re} \left(\frac{1}{\sqrt{\cos \theta + s_1 \sin \theta}} + \frac{1}{\sqrt{\cos \theta + s_2 \sin \theta}} \right) - \beta \operatorname{Im} \left(\frac{1}{\sqrt{\cos \theta + s_1 \sin \theta}} - \frac{1}{\sqrt{\cos \theta + s_2 \sin \theta}} \right) \right]
 \end{aligned} \tag{40}$$

2. Solution by Lekhnitskii's Method [4][9] *

Returning to Eq. (11)

$$U = Z_1(\xi_1) + Z_2(\bar{\xi}_1) + Z_3(\xi_2) + Z_4(\bar{\xi}_2) \quad (11)$$

where ξ_1, ξ_2 are defined by Eq. (13).

Corresponding to the stress function $U = \text{Re} \left[\bar{z} \Phi(z) - \chi(z) \right]$ in the isotropic case, the stress function for Eq. (11) is

$$U = 2 \text{Re} \left[Z_1(\xi_1) + Z_2(\xi_2) \right]. \quad (41)$$

The following additional notations are introduced:

$$\frac{dZ_1}{d\xi_1} = \bar{\Phi}_1(\xi_1); \quad \frac{d}{d\xi_1} = \bar{\Phi}'_1(\xi_1), \quad (42)$$

$$\frac{dZ_2}{d\xi_2} = \bar{\Phi}_2(\xi_2); \quad \frac{dZ_2}{d\xi_2} = \bar{\Phi}'_2(\xi_2).$$

Substitution of (41) into (5) using (42) gives

$$\begin{aligned} \sigma_x &= 2 \text{Re} \left[s_1^2 \bar{\Phi}'_1(\xi_1) + s_2^2 \bar{\Phi}'_2(\xi_2) \right], \\ \sigma_y &= 2 \text{Re} \left[\bar{\Phi}'_1(\xi_1) + \bar{\Phi}'_2(\xi_2) \right], \\ \tau_{xy} &= -2 \text{Re} \left[s_1 \bar{\Phi}'_1(\xi_1) + s_2 \bar{\Phi}'_2(\xi_2) \right]. \end{aligned} \quad (43)$$

Lekhnitskii gives the stress functions $\bar{\Phi}_1(\xi_1), \bar{\Phi}_2(\xi_2), \bar{\Phi}_3(\xi_3)$ for an anisotropic space containing an elliptical cylindrical cavity under arbitrary external tractions. The stress functions can be modified for a plane containing an elliptical hole. Performing the necessary operations, the stress functions for the plane problem are:

$$\begin{aligned} \bar{\Phi}_1(\xi_1) &= A_1 \ln \eta_1 + \frac{1}{s_1 - s_2} \sum_{m=1}^{\infty} (\bar{b}_m - s_2 \bar{a}_m) \eta_1^{-m}, \\ \bar{\Phi}_2(\xi_2) &= A_2 \ln \eta_2 - \frac{1}{s_1 - s_2} \sum_{m=1}^{\infty} (\bar{b}_m - s_1 \bar{a}_m) \eta_2^{-m}, \\ \bar{\Phi}_3(\xi_3) &= 0. \end{aligned} \quad (44)$$

* In the following brief summary of Lekhnitskii's method, most of the notations of the original author are retained. However, some of the notations are changed in order to relate the corresponding terms which appeared previously in the analysis obtained by the Westergaard-Irwin type of solution.

where

$$\eta_k = \frac{\xi_k + \sqrt{\xi_k^2 - a^2 - s_k^2 b^2}}{a - i s_k b} \quad k = 1, 2 \quad (45)$$

and a is the major axis and b is the minor axis of the ellipse.

For a crack of length $2a$ instead of an elliptical hole, the η_k in the stress functions $\bar{\Phi}_1$ and $\bar{\Phi}_2$ take on the special values for $b = 0$, i. e.

$$\eta_k = \frac{\xi_k + \sqrt{\xi_k^2 - a^2}}{a} \quad k = 1, 2 \quad (46)$$

Using the notations defined by Eq. (42) and letting $b = 0$, Eq. (44) becomes

$$\begin{aligned} \bar{\Phi}'_1(\xi_1) &= \frac{1}{\sqrt{\xi_1^2 - a^2}} A_1 - \frac{1}{s_1 - s_2} \sum_{m=1}^{\infty} m(\bar{b}_m - s_2 \bar{a}_m) \eta_1^{-m}, \\ \bar{\Phi}'_2(\xi_2) &= \frac{1}{\sqrt{\xi_2^2 - a^2}} A_2 + \frac{1}{s_1 - s_2} \sum_{m=1}^{\infty} m(\bar{b}_m - s_1 \bar{a}_m) \eta_2^{-m}. \end{aligned} \quad (47)$$

For the loading condition as shown in Fig. 2a Lekhnitskii* indicated that the constants in Eq. (47) are

$$\begin{aligned} \bar{a}_1 &= -\frac{a\sigma}{2}, \\ \bar{b}_1 &= 0, \\ \bar{a}_m = \bar{b}_m &= 0 \quad m \geq 2, \\ A_1 = A_2 &= 0. \end{aligned}$$

For the loading condition as shown in Fig. 2b, the constants are

$$\begin{aligned} \bar{a}_1 &= 0, \\ \bar{b}_1 &= \frac{a\tau}{2}, \\ \bar{a}_m = \bar{b}_m &= 0 \quad \text{for } m \geq 2, \\ A_1 = A_2 &= 0. \end{aligned}$$

* This is obtained by reducing the results of Ref. [9] pp. 129-131 to a plane problem and taking the special case of a degenerate ellipse (i. e. the minor axis $b = 0$). Similar results can be obtained from Savin's work Ref. [4] pp. 157-162.

For the loading condition as shown in Fig. 2c, superimposing the two results gives the constants in Eq. (47):

$$\begin{aligned}\bar{a}_1 &= -\frac{a\sigma}{2}, \\ \bar{b}_1 &= \frac{a\tau}{2}, \\ \bar{a}_m &= \bar{b}_m = 0 \text{ for } m \geq 2, \\ A_1 &= A_2 = 0.\end{aligned}$$

Substitution of Eqs. (47) and (48) into Eq. (43) gives the stress distribution in the plate under the loading conditions as indicated in Fig. 2c:

$$\begin{aligned}\sigma_x &= \text{Re} \left\{ \frac{a}{(s_1 - s_2)} \left[\frac{-s_1^2(\tau + s_2\sigma)}{\eta_1 \sqrt{\xi_1^2 - a^2}} + \frac{s_2^2(\tau + s_1\sigma)}{\eta_2 \sqrt{\xi_2^2 - a^2}} \right] \right\}, \\ \sigma_y &= \text{Re} \left\{ \frac{a}{(s_1 - s_2)} \left[\frac{-(\tau + s_2\sigma)}{\eta_1 \sqrt{\xi_1^2 - a^2}} + \frac{(\tau + s_1\sigma)}{\eta_2 \sqrt{\xi_2^2 - a^2}} \right] \right\}, \\ \tau_{xy} &= -\text{Re} \left\{ \frac{a}{(s_1 - s_2)} \left[\frac{-s_1(\tau + s_2\sigma)}{\eta_1 \sqrt{\xi_1^2 - a^2}} + \frac{s_2(\tau + s_1\sigma)}{\eta_2 \sqrt{\xi_2^2 - a^2}} \right] \right\}.\end{aligned}\quad (49)$$

To consider the stress intensity at the vicinity of the tip of the crack where $r \ll a$, the same simplifications as discussed in section II B 1 can be made. Using Eq. (27)

$$\eta_1 = \eta_2 = 1 \text{ when } r \ll a.$$

Then the crack tip stress distribution obtained by Lekhnitskii's method is *

$$\begin{aligned}\sigma_x &= \frac{\sqrt{a}}{\sqrt{2r}} \text{Re} \left\{ \frac{1}{(s_1 - s_2)} \left[\frac{-s_1^2(\tau + s_2\sigma)}{\sqrt{\cos \theta + s_1 \sin \theta}} + \frac{s_2^2(\tau + s_1\sigma)}{\sqrt{\cos \theta + s_2 \sin \theta}} \right] \right\}, \\ \sigma_y &= \frac{\sqrt{a}}{\sqrt{2r}} \text{Re} \left\{ \frac{1}{(s_1 - s_2)} \left[\frac{-(\tau + s_2\sigma)}{\sqrt{\cos \theta + s_1 \sin \theta}} + \frac{(\tau + s_1\sigma)}{\sqrt{\cos \theta + s_2 \sin \theta}} \right] \right\}, \\ \tau_{xy} &= \frac{\sqrt{a}}{\sqrt{2r}} \text{Re} \left\{ \frac{1}{(s_1 - s_2)} \left[\frac{s_1(\tau + s_2\sigma)}{\sqrt{\cos \theta + s_1 \sin \theta}} - \frac{s_2(\tau + s_1\sigma)}{\sqrt{\cos \theta + s_2 \sin \theta}} \right] \right\}.\end{aligned}\quad (50)$$

* G. C. Sih and P. C. Paris [10] discussed a similar problem solved by Lekhnitskii. However the result given by Sih and Paris is contradictory to that given here in the respect that the roles of σ and τ are reversed in addition to some sign discrepancies.

3. Comparison of the Two Solutions

It should be noted that both Eq. (40) and Eq. (50) describe the stress distribution around the tip of a crack in an infinite orthotropic plate. From physical consideration, the stresses in Eq. (40) and Eq. (50) are necessarily real. This indeed is the case since the real and imaginary parts of the complex variables in the expressions are real quantities.

Further, both of the expressions are simplified by neglecting r terms of order higher than $r^{-1/2}$. Therefore from the uniqueness theorem in the theory of elasticity, Eq. (40) and Eq. (50) should be identical. Although little similarity can be noted in their present forms, they can be compared by expressing the real and imaginary parts differently as follows:

$$\begin{aligned} \frac{1}{\sqrt{\cos \theta + s_1 \sin \theta}} &= \frac{1}{\sqrt{(\cos \theta + \alpha \sin \theta) + i (\beta \sin \theta)}} \\ &= \frac{1}{\sqrt{(\cos \theta + \alpha \sin \theta)^2 + (\beta \sin \theta)^2}} \left(\cos \frac{\phi_1}{2} - i \sin \frac{\phi_1}{2} \right) \end{aligned} \quad (51)$$

where

$$\begin{aligned} \sin \phi_1 &= \frac{\beta \sin \theta}{\sqrt{(\cos \theta + \alpha \sin \theta)^2 + (\beta \sin \theta)^2}}, \\ \cos \phi_1 &= \frac{\cos \theta + \alpha \sin \theta}{\sqrt{(\cos \theta + \alpha \sin \theta)^2 + (\beta \sin \theta)^2}}; \end{aligned} \quad (52)$$

similarly

$$\frac{1}{\sqrt{\cos \theta + s_2 \sin \theta}} = \frac{1}{\sqrt{(\cos \theta - \alpha \sin \theta)^2 + (\beta \sin \theta)^2}} \left(\cos \frac{\phi_2}{2} - i \sin \frac{\phi_2}{2} \right) \quad (53)$$

where

$$\begin{aligned} \sin \phi_2 &= \frac{\beta \sin \theta}{\sqrt{(\cos \theta - \alpha \sin \theta)^2 + (\beta \sin \theta)^2}}, \\ \cos \phi_2 &= \frac{\cos \theta - \alpha \sin \theta}{\sqrt{(\cos \theta - \alpha \sin \theta)^2 + (\beta \sin \theta)^2}}. \end{aligned} \quad (54)$$

Using Eqs. (51) to (54), it can be shown that Eq. (40) and Eq. (50) are identical and they can both be expressed as

$$\begin{aligned} \sigma_x &= \frac{\sigma\sqrt{a}}{\sqrt{2r}} \left(\frac{\alpha^2 + \beta^2}{2\alpha} \right) \left[\frac{\alpha \cos \frac{\phi_1}{2} + \beta \sin \frac{\phi_2}{2}}{\sqrt{(\cos\theta + \alpha \sin\theta)^2 + (\beta \sin\theta)^2}} + \frac{\alpha \cos \frac{\phi_2}{2} - \beta \sin \frac{\phi_2}{2}}{\sqrt{(\cos\theta - \alpha \sin\theta)^2 + (\beta \sin\theta)^2}} \right] \\ &\quad - \frac{\tau\sqrt{a}}{\sqrt{2r}} \left(\frac{1}{2\alpha} \right) \left[\frac{(\alpha^2 - \beta^2) \cos \frac{\phi_1}{2} + 2\alpha \beta \sin \frac{\phi_1}{2}}{\sqrt{(\cos\theta + \alpha \sin\theta)^2 + (\beta \sin\theta)^2}} - \frac{(\alpha^2 - \beta^2) \cos \frac{\phi_1}{2} + 2\alpha \beta \sin \frac{\phi_2}{2}}{\sqrt{(\cos\theta - \alpha \sin\theta)^2 + (\beta \sin\theta)^2}} \right], \\ \sigma_y &= \frac{\sigma\sqrt{a}}{\sqrt{2r}} \left(\frac{1}{2\alpha} \right) \left[\frac{\alpha \cos \frac{\phi_1}{2} - \beta \sin \frac{\phi_1}{2}}{\sqrt{(\cos\theta + \alpha \sin\theta)^2 + (\beta \sin\theta)^2}} + \frac{\alpha \cos \frac{\phi_2}{2} + \beta \sin \frac{\phi_2}{2}}{\sqrt{(\cos\theta - \alpha \sin\theta)^2 + (\beta \sin\theta)^2}} \right] \\ &\quad - \frac{\tau\sqrt{a}}{\sqrt{2r}} \left(\frac{1}{2\alpha} \right) \left[\frac{\cos \frac{\phi_1}{2}}{\sqrt{(\cos\theta + \alpha \sin\theta)^2 + (\beta \sin\theta)^2}} - \frac{\cos \frac{\phi_1}{2}}{\sqrt{(\cos\theta - \alpha \sin\theta)^2 + (\beta \sin\theta)^2}} \right], \end{aligned} \quad (55)$$

$$\begin{aligned} \tau_{xy} &= - \frac{\sigma\sqrt{a}}{\sqrt{2r}} \left(\frac{\alpha^2 + \beta^2}{2\alpha} \right) \left[\frac{\cos \frac{\phi_1}{2}}{\sqrt{(\cos\theta + \alpha \sin\theta)^2 + (\beta \sin\theta)^2}} - \frac{\cos \frac{\phi_2}{2}}{\sqrt{(\cos\theta - \alpha \sin\theta)^2 + (\beta \sin\theta)^2}} \right] \\ &\quad + \frac{\tau\sqrt{a}}{\sqrt{2r}} \left(\frac{1}{2\alpha} \right) \left[\frac{\alpha \cos \frac{\phi_1}{2} + \beta \sin \frac{\phi_1}{2}}{\sqrt{(\cos\theta + \alpha \sin\theta)^2 + (\beta \sin\theta)^2}} + \frac{\alpha \cos \frac{\phi_2}{2} - \beta \sin \frac{\phi_2}{2}}{\sqrt{(\cos\theta - \alpha \sin\theta)^2 + (\beta \sin\theta)^2}} \right] \end{aligned}$$

where ϕ_1 and ϕ_2 are defined by Eq. (52) and (54).

In general, arbitrary external plane tractions can be resolved in terms of σ_1 , σ_2 and τ as shown in Fig. 1b. However, it can be shown [4] that the stress distribution in an anisotropic plate is not influenced by a straight crack in the direction of the tensile stress. In other words, the component of tensile traction in the direction of a crack does not contribute to the stress singularity at the crack tip and its effect on the stability of the crack is small and can be neglected. Consequently Fig. 2 c, in fact, represents the general case of plane loading in the absence of bending and twisting. For a thin orthotropic plate containing a single crack in the direction of one of its two axes of elastic symmetry under an arbitrary external tractions, Eqs. (55) gives the stress distribution around the tip of the crack.

C. Comparison of the Crack Tip Stress Distribution in an Orthotropic Plate to that in an Isotropic Plate.

For an isotropic plate containing a single crack under the loading condition as shown in Fig. 2c, and after neglecting r terms of order high than $r^{1/2}$, the crack tip stress distribution can be expressed as

$$\begin{aligned}
 \sigma_x &= \frac{\sigma\sqrt{a}}{\sqrt{2r}} \cos \frac{\theta}{2} \left(1 - \sin \frac{\theta}{2} \sin \frac{3\theta}{2} \right) \\
 &\quad - \frac{\tau\sqrt{a}}{\sqrt{2r}} \sin \frac{\theta}{2} \left(2 + \cos \frac{\theta}{2} \cos \frac{3\theta}{2} \right), \\
 \sigma_y &= \frac{\sigma\sqrt{a}}{\sqrt{2r}} \cos \frac{\theta}{2} \left(1 + \sin \frac{\theta}{2} \sin \frac{3\theta}{2} \right) \\
 &\quad + \frac{\tau\sqrt{a}}{\sqrt{2r}} \sin \frac{\theta}{2} \cos \frac{\theta}{2} \cos \frac{3\theta}{2}, \\
 \tau_{xy} &= \frac{\sigma\sqrt{a}}{2r} \sin \frac{\theta}{2} \cos \frac{\theta}{2} \cos \frac{3\theta}{2} \\
 &\quad + \frac{\tau\sqrt{a}}{\sqrt{2r}} \cos \frac{\theta}{2} \left(1 - \sin \frac{\theta}{2} \sin \frac{3\theta}{2} \right),
 \end{aligned} \tag{56}$$

where the stress intensity factors are

$$\begin{aligned}
 k_1 &= \sigma\sqrt{a} \quad (\text{symmetric}), \\
 k_2 &= \tau\sqrt{a} \quad (\text{skew-symmetric}).
 \end{aligned}$$

Comparison of Eq. (55) to Eq. (56), leads to the following observations. The most obvious difference between the state of stress in the vicinity of the tip of a crack in an orthotropic plate and that in an isotropic plate is that the former is dependent on the elastic constants of the material* while the latter is not. However, there are also several similarities. First, the stress singularity at the tips of the crack (r approaching zero) for both cases is of the order $r^{-1/2}$. Second, a parameter characterizing the effect of the size of the crack and the magnitude of the external stress for the ortho-

* The quantities α , β , ϕ_i are functions of E_x , E_y , ν_x , ν_y and G_{xy} .

tropic plate can be defined in a manner similar to the isotropic case, namely,

$$\begin{aligned} k_1 &= \sigma\sqrt{a}, \\ k_2 &= \tau\sqrt{a}. \end{aligned} \tag{57}$$

The stress intensity factors, k_1 and k_2 therefore can be used as parameters to measure the strength of a cracked orthotropic plate. The crack extension force, \mathcal{G}_1 and \mathcal{G}_2 obtained from energy considerations by Irwin [2] are generally considered to be more fundamental parameters related to crack extension. However, in order to obtain \mathcal{G}_1 and \mathcal{G}_2 , a knowledge of the direction of the crack growth is necessary. In an isotropic material a generally accepted hypothesis which postulates that crack growth is perpendicular to the direction of greatest tension has been verified experimentally. However, no such hypothesis is possible for orthotropic materials since the direction of crack growth depends on the strength of the material as well as the state of stress. Due to this difficulty, the crack instability of orthotropic plates will be examined using the stress intensity factors as criteria.

Defining k_{1c} and k_{2c} as the critical magnitude of the stress intensity factors for unstable crack extension under simple tension and under pure shear respectively, the combined influence of stress-intensity factors can be expressed in the following form:

$$\left(\frac{k_1}{k_{1c}}\right)^m + \left(\frac{k_2}{k_{2c}}\right)^n = 1. \tag{58}$$

Obviously, in order to express k_{1c} and k_{2c} in a functional relationship, a fracture criterion relating the influence of symmetric and skew-symmetric loading for orthotropic material is required. At present, not only is a fracture criterion of this type unavailable for orthotropic materials, but a workable criterion has yet to be formulated and validated for homogeneous isotropic materials. Consequently the exponents m and n in Eq. (58) must be determined experimentally. From the experimental results, a suitable fracture criterion for orthotropic material may become evident.

III. EXPERIMENTAL PROGRAM

A. Introduction to the Experimental Investigation

1. Purpose of the Experimental Program

An experimental program was designed to determine the validity of the hypothesis formulated from the analytical results. There are two main objectives to the experimental program for orthotropic plates: (a) To investigate the feasibility of using stress intensity factors k_1 and k_2 as criteria for unstable crack extension, and (b) To investigate if a functional relation between k_1 and k_2 exists and, if it does exist, whether it can be expressed in the form of Eq. (58).

The material chosen for the experimental investigation was balsa wood. This choice was based on two factors: first because it was essentially orthotropic, and second because it was readily available and suitable specimens could be easily prepared and tested. However, due to the non-uniformity of the wood* only a qualitative demonstration of the fracture mechanics to orthotropic plates should be expected.

2. Experimental Set-up

In these experiments, the desired loading can be classified into three types: (a) Pure tension perpendicular to the crack, (b) Pure shear and (c) Combined tension and shear. Two methods of testing were used to achieve these loading conditions.

In the first method of testing, the tension test as shown in Fig. 3a, loading from pure tension perpendicular to the crack to combined tension and shear can be obtained by varying the relative angle γ between the applied tension and the line of the crack **. The specimen was gripped at opposite ends, one end being pinned to a table and allowed to rotate. The tension load was transferred to the other grip through a long cable to minimize any bending moment induced by the deformation of the specimen. However, pure shear could not be obtained by this method. Consequently a second loading method was used.

A dead-weight testing machine shown in Fig. 5 was constructed to load the specimen in pure shear as well as in combined tension and shear. Its essential components are shown in the schematic drawing in Fig. 6. A square balsa wood specimen was gripped on all four sides. Grip No. 1 was pinned to the machine base so that rotation in the plane of the plate was possible. Cables connected to the remaining three grips

* This will be discussed in a later section.

** Since it has been noted in section II B 3 that tension in the direction of the crack has no effect on the stress singularity at the crack tip, σ_x in Fig. 3a need not be considered and the loading condition can be considered to be identical to that represented in Fig. 2c.

were arranged as shown in Fig. 6; the three cables were then connected together in a manner such that the load on a single center pin was distributed equally to each of the three cables. These loads combined with the reaction force from the pin applied a pure shear to the specimen. The load transferring cables were of sufficient length so that the pure shear condition remained unaffected when the specimen deformed under load. For tension, another cable was attached to grip No. 2 (in Fig. 6) and loaded by a separate weight. The detailed manner in which the cables were connected to the grips is shown in Fig. 7. Note that the pin (A) was located in the center of the gripping area so that no moment was produced. The construction of the grips is also shown in Fig. 7. Each grip was assembled from two aluminum pieces. The gripping surfaces were made of pads of rubber which has an elastic modulus close to that of the balsa wood thus minimizing the constraint of the grips. By means of a torque wrench, a minimum tightening force required to prevent the grips from slipping under load was determined and maintained uniformly from specimen to specimen.

To prevent buckling in shear, the grips were constrained in a plane by two plates of glass. Plexiglass plates were affixed to the glass plates to further constrain the specimen from buckling. A cross-sectional view indicating their relative position is shown in Fig. 8. The clearance between the plexiglass plates and the specimens was approximately 0.005 in. The friction between the aluminum grips and the glass plates was very small and the displacement of the grips was not significantly restricted.

Observation of the crack was facilitated by placing a light below the specimen. The crack length was measured using a traveling microscope of 20X power to which a vernier scale was attached thus providing length measurements accurate to 0.01 inch, Fig. 5 and 8.

B. Testing Procedure

The stress analysis presented in Part I is applicable to a single crack parallel to one of the principle planes of elastic symmetry of a large plate. In these experiments, only the case of a crack parallel to the grain of the balsa wood was investigated since it is the most frequently observed mode of cracking in orthotropic plates.

Four different combinations of load were employed. Referring to Fig. 9, path No. 1 represents tension perpendicular to the crack. Path No. 2 represents a crack orientated at an angle γ to the line of tension. Path No. 3 represents a specimen loaded first to a pure tension stress, σ_0 , and then loaded to fracture by increasing the shear stress. Path No. 4 represents pure shear loading. As stated in the previous section, two types of testing methods were used: first a tension test with the crack orientated at

various angles with respect to the line of tension and second a pure shear test or combined tension and shear test using four grips to apply the desired loads. Since different procedures for the two types of testing are used, they will be discussed separately.

1. Tension Tests (Path No. 1 and 2)

Five groups of specimens were tested in tension. The dimensions and the values of the angle γ for each group are listed in the table below.

Group	γ -deg	Thickness in	Width in	Length in
1	90 ⁰	1/16	6	6
2	65 ⁰	1/16	4-1/2	6
3	50 ⁰	1/16	4-1/2	6
4	35 ⁰	1/16	4-1/2	8-1/2
5	20 ⁰	1/16	4	14

The variations in dimensions of the specimens were dictated by two considerations: (a) The longer lengths were provided for small values of γ so as to prevent crack propagation into the grips, (b) The narrower widths of the specimens were necessitated by the size of the balsa wood plate available.

An initial crack was put in the center of the specimen which was clamped in the grips and loaded in tension by dead-weights. The crack length was measured using the microscope, and the load increments at which crack length measurements were made were large at low loads and reduced accordingly when the crack length was observed to increase. This procedure was continued until fracture occurred. After the specimen was fractured, it was observed that the crack usually did not propagate at the original angle γ , but at a slightly different angle. The actual angle of fracture of the region near the center of the specimen was measured. From this angle, the component of tension stress σ perpendicular to the crack and the shear stress component τ were computed. Typical results of the experiments are shown in Fig. 10 and 11 where the observed crack lengths $2a$ are plotted as abscissa corresponding to the value of σ or τ , shown as ordinates. These results will be discussed later.

2. Combined Tension and Shear and Pure Shear Tests (Path No. 3 and 4)

In the second series of tests, all of the specimens had dimensions of 6" x 6" x 1/16". From the construction of the testing machine, it was clear that the side grips, No. 3 and 4 in Fig. 6, must be in place in order to apply shear load. However, if tension load was applied after the side grips were in place, these side grips would constrain the elongation of the specimen. Consequently in the combined tension

and shear tests which follow path No. 3 a different procedure was used. For each group of specimens, the tension stress was increased to the desired level with the side-grips absent. Then the side grips, No. 3 and 4, were put in place and shear load was increased while the crack length was measured at increments up to fracture. Four such groups of specimens were tested for constant tension stress of 25, 48.6, 62 and 71 psi respectively. The typical relations of τ vs $2a$ observed at constant σ are shown in Fig. 12.

In the pure shear test, a crack was located in the center of the specimen parallel to the wood grain and its length was measured at appropriate load increments. A typical diagram of τ vs $2a$ is presented in Fig. 13.

C. Interpretation of Data and Results

In the experimental investigation, it was observed that in almost all cases, some stable crack extension took place prior to the sudden fracture of a specimen. The amount of stable crack extension, the load level at which the crack began to extend, and the rate of extension all vary from specimen to specimen. Slight variations in the properties of the wood are believed to be the cause of these differences. Cracks in the majority of the specimens tend to start extending at approximately 85% of the load level at which rapid fracture occurs. Typical data for specimens No. 52, 110 and 44 are shown in Fig. 10, 11 and 13 respectively. Other frequently observed crack extension patterns are described below.

A crack which was located in a low density region of the wood normally extended much more than one located in a higher density region. Examples of each type of behavior are specimens No. 105 and 41 shown in Fig. 11 and 13. Sometimes, a defect in the wood was located near the tip of the crack. In this case, the crack began to extend at a low load level, but stopped after it had propagated through the defective region. This crack remained at a constant length until the fracture load was approached when it again resumed the normal extension pattern to fracture. Specimen No. 14 in Fig. 12 is a typical example of this pattern of crack extension. Another irregularity observed was an obstacle which appeared in the microscope as a dark spot located in the path of the crack. An extraordinarily high stress level was required for the crack to overcome the obstacle. On the other hand, a very low fracture stress resulted when the crack extended into a large weak region such as a long weak grain. However, the worst irregularities were avoided by judicious placement of the crack in a grossly homogeneous region by examining the specimen in front of a strong light source.

Since the purpose of the experiments was to investigate the unstable crack propa-

gation phenomena, the desired information was the stress level and crack length at which the crack propagated rapidly to fracture. Because various crack extension patterns were observed, a suitable convention was required so that the critical stress level and the critical crack length could be defined. The stress at fracture was defined as the critical stress level. On diagrams of σ vs $2a$ or τ vs $2a$, a straight line was drawn tangent to the last measured stable crack length and its intercept with the critical stress level was defined as the critical crack length. In effect, this definition of critical crack length assumed that the stable crack extension rate was unchanged from the last measurement up to the point of fracture. This assumption was reasonable because the last incremental increase of load was usually very small as can be observed from the graphs.

As stated earlier the fracture angles in the tension tests often differed slightly from the original crack orientation angle. This variation was observed in each group of tests. To account for this, the arithmetic mean of the final fracture angles of all specimens tested in each group was computed and denoted by γ_{mean} . The results of each group of specimens are shown on diagrams of $\log \sigma$ vs $\log a$ or $\log \tau$ vs $\log a$. Referring to the loading paths in Fig. 9, the results of tests which follow path No. 1 is presented in Fig. 14, and the results of the tests which follow path No. 4 is presented in Fig. 15. The results of path No. 2 at γ_{mean} equal to 64° , 50° , 35.5° and 22° are presented in Fig. 16a and b, 17a and b, 18a and b, 19a and b, respectively. Finally, the results of path No. 3 at constant tension stress σ_0 equal to 25, 48.6, 62, and 71 psi are presented in Fig. 20, 21, 22, and 23 respectively.

D. Discussion of Results

In the analysis of stress in the vicinity of the tips of a crack, it was suggested that the stress intensity factors k_1 and k_2 could be used as parameters to measure the strength of an orthotropic plate containing a crack. If this is feasible (as it is in the isotropic case) the critical stress intensity factors k_{1c} and k_{2c} could be constants for one orthotropic material. Equation (57) can be written in the following form:

$$\begin{aligned}\log k_{1c} &= \log \sigma + \frac{1}{2} \log a, \\ \log k_{2c} &= \log \tau + \frac{1}{2} \log a.\end{aligned}\tag{59}$$

If k_{1c} and k_{2c} are constants, then Eq. (59) suggests a linear relation between $\log \sigma$ and $\log a$ or $\log \tau$ and $\log a$ with slope equal to -0.5 on log-log plots.

In order to examine the hypothesis that the experimental results represent a

straight line of slope equal to -0.50 , the data obtained from the tests which follow path No. 1 are presented in Fig. 14. The σ_{mean} and a_{mean} of all of the experimental data were computed and are indicated in Fig. 14 by a cross (x). Next the mean of the data in the region $a < a_{\text{mean}}$ and similarly the mean of the data in the region $a > a_{\text{mean}}$ (indicated by two solid dots) were located. If a straight line passes through the three points, it is reasonable to conclude that these data may be represented by a straight line. In Fig. 14 it can be seen that the three points fall on a straight line the slope of which was determined graphically to be -0.47 . However, since a slope of -0.5 was predicted by the analysis, a line of this slope was drawn through the mean. A band of ± 10 per cent about this line included almost all of the experimental data. Within the realm of experimental scatter, the critical stress intensity factor $k_{1c} = \sigma \sqrt{a} = \text{constant}$ provided a good description of the data for orthotropic plates tested under loading symmetrical to a crack.

In the same manner, the results of the pure shear experiments which are presented in Fig. 15 were analyzed, and these data also were well represented by a straight line with a slope equal to -0.48 . Again a band of ± 10 per cent about the line of -0.5 slope through the mean included most of the data. Consequently, it was concluded that the critical stress intensity factor $k_{2c} = \tau \sqrt{a} = \text{constant}$ is likewise applicable to orthotropic plates tested under loading skew symmetrical to a crack.

In the tests which followed path No. 2 where a tension load was applied at an angle γ to the crack, the tension component σ perpendicular to the crack and the shear component τ were calculated from the actual fracture angle of each specimen. If the fracture angles of the specimens in each group were the same then the ratio of σ/τ would have been constant. But, since these fracture angles varied slightly from specimen to specimen in the same group, it is evident from Mohr's circle that the ratio of σ/τ is not constant and the data would be distributed differently in the graphs of $\log \sigma$ vs $\log a$ than the data represented in the graphs $\log \tau$ vs $\log a$. Thus it is necessary that the data be represented in both of these graphs, and they are presented in Figs. 16 to 19. The measured mean fracture angles, the number of specimens and the slopes of straight lines estimated from these data are summarized in the following table.

Original Angle	Mean Angle of Fracture	No. of Specimens Tested	$k_1 = (a)^h \sigma$	$k_2 = (a)^\ell \tau$
γ	γ_{mean}	N	h	ℓ
65°	64°	8	-.65	-.57
50°	50°	7	-.40	-.43
35°	35.5°	12	-.55	-.53
20°	22°	10	-.40	-.46

Because of the increased scatter and the relatively few data points, the straight lines that were estimated from the data exhibited slopes h and ℓ which differed measurably from -0.50 . However further examination of the data revealed that the slopes of those lines which were determined from the larger number of data points were closer to -0.50 . Furthermore, the average values of h and ℓ of the four groups of tests were both very nearly equal to -0.50 . Therefore it appeared that as the number of data points were increased, the slope of the straight line determined by these data would closely approach -0.50 . Within the realm of the accuracy of the experiments, straight lines of slope equal to -0.50 were drawn through the point determined by σ_{mean} and a_{mean} (indicated by a cross) in each figure. A band enclosing a region ± 10 per cent about the mean line included a majority of the data. Thus these data provide additional evidence that a straight line of slope -0.50 was a good description of the relation between $\log \sigma$ and $\log a$ and between $\log \tau$ and $\log a$ as suggested by Eq. (59). From these data, two important conclusions emerge regarding an orthotropic plate which contains a crack and is tested under combined tension σ and shear τ . First, the stress intensity factors $k_1 = \sigma\sqrt{a}$ and $k_2 = \tau\sqrt{a}$ provide a good description of the relation between σ and a , and τ and a for rapid crack extension. Second, various combinations of k_1 and k_2 may be considered as critical combinations which produce unstable crack extension to fracture. Thus these data suggest that a function $f(k_1, k_2) = f_{\text{critical}}$ exists, which describes the conditions for unstable fracture.

The results of the combined tension and shear experiments which followed path No. 3 are presented in Fig. 20 to 23. For combined tension and shear, the critical stress intensity factor $k_{1c} = \sigma\sqrt{a}$ for rapid crack extension had been shown to be a constant. Thus for experiments described by path No. 3, if σ is constant, then k_1 cannot be constant. Therefore the data of the tests which followed path No. 3 representing $\log \tau$ as a function of $\log a$ do not produce a straight line, but rather, a curve representing $f(k_1, k_2) = f_{\text{critical}}$.

To examine the function $f(k_1, k_2) = f_{\text{critical}}$, that is the interaction between k_1 and k_2 under combined loadings, the values of k_1 and k_2 are needed. Since the relations

$k_1 = \sigma\sqrt{a}$ and/or $k_2 = \tau\sqrt{a}$ were applicable for all loading conditions, tension, pure shear and combinations of tension and shear, the values of k_1 and k_2 for all of the experimental data were computed. These values are shown in Fig. 24 where k_1 is the ordinate and k_2 is the abscissa. The data in Fig. 24 define the functional relationship between k_1 and k_2 corresponding to unstable crack extension. A curve is drawn through the points to represent the function $f(k_1, k_2) = f_c$, with end points for tension $f(k_1, 0) = k_{1c}$ and for pure shear $f(0, k_2) = k_{2c}$. A band which represents the maximum deviation from the mean curve resulting simultaneously from $k_1 \pm 10$ per cent and $k_2 \pm 10$ per cent is also indicated. For the purpose of illustration this average curve and the deviation band are replotted in Fig. 20 to 23.

To obtain the function $f(k_1, k_2) = f_c$, a dimensionless representation was used. Using the curve in Fig. 24 which represents the average of the experimental data, a graph of k_1/k_{1c} vs k_2/k_{2c} is plotted in Fig. 25. The curve relating k_1 and k_2 was assumed in the form of Eq. (58):

$$\left(\frac{k_1}{k_{1c}}\right)^m + \left(\frac{k_2}{k_{2c}}\right)^n = 1.$$

The exponents m and n were determined by choosing two points on the curve in Fig. 25. Substituting these into Eq. (62) led to two simultaneous equations from which m and n were obtained. This procedure was repeated several times using different pairs of points on this curve until an average value of m and n was obtained. The values of m and n which were found to fit the experimental data were

$$\begin{aligned} m &= 1.03, \\ n &= 1.88. \end{aligned}$$

The important features of this function with the above values of m and n are that the exponents m and n are not equal, and the function is defined only in the domain $k_1 \geq 0$ and $k_2 \geq 0$ since m and n are not integers. Referring to Fig. 26, it can be seen that $f(k_1, k_2) = f_c$ is necessarily even in k_2 , i. e. $f_c(k_1, -k_2) = f_c(k_1, k_2)$ because the direction of shear is arbitrary. Furthermore under combined compression and shear, the curve $f(k_1, k_2) = f_c$ is likely to extend along the broken line shown in Fig. 26. To meet these physical requirements, the exponents $m = 1$, $n = 2$ were chosen. This gave a function that is even in k_2 and defined for $k_1 > 0$ as well as $k_1 < 0$. Then Eq. (58) becomes

$$\left(\frac{k_1}{k_{1c}}\right) + \left(\frac{k_2}{k_{2c}}\right)^2. \quad (60)$$

Equation (60), which is shown by the broken curves in Fig. 24 and 25 defines a curve that is not significantly different from the average experimental curve. This equation fits the data excellently and satisfies the above mentioned physical considerations. Consequently, Eq. (60) was used to represent the function $f(k_1, k_2) = f_c$ for the balsa wood sheets tested.

E. Discussion of Experimental Accuracy

The major sources of error in the experimental investigation were; 1. The non-uniformity of the balsa wood used for specimens. 2. The accuracy of the crack measurements. 3. The constraint introduced by the side grips in the combined tension and shear tests. 4. Buckling of the specimen under shear. 5. Absolute similitude was not maintained between the theoretical model in the analysis and the model used for experimental investigation. These sources of error will be considered separately.

1. The non-uniformity of the balsa wood used for specimens. The non-uniformity of wood can be classified into two types, first, localized non-homogeneity of wood which probably caused the different crack extension patterns described in section III C and second, discrete macroscopic regions of different densities within a specimen as shown by the light and dark bands in the picture of a typical specimen in Fig. 4a.

It was found that by examining the specimen in front of a strong light source, the non-homogeneous regions could be observed and the density of the wood could be compared. Using this technique, balsa wood sheets which showed approximately the same uniform density in the prospective crack regions were chosen for testing. This method of choosing specimens eliminated the major variations in wood. An investigation was designed to determine the influence of the specific gravity on the fracture strength of the balsa wood specimens.

Since discrete regions of different densities exist within a specimen, it is the specific gravity in the immediate vicinity of the crack rather than the average specific gravity of the entire specimen that should be examined. After a specimen had been tested, strips of wood approximately 1/4" wide on each side of the fracture surfaces were cut out and the specific gravity of these two strips were measured. This method of specific gravity measurement was applied to specimens which were tested in tension perpendicular to the crack and those tested in pure shear. The deviation from the mean specific gravity was denoted by $\Delta S.G.$. The deviation of the critical stress intensity factor of each specimen from the respective means are denoted by Δk_c . A plot of Δk_c vs $\Delta S.G.$ is shown in Fig. 27 where the solid points and open points represent

data obtained from the tension test and pure shear test respectively. In this figure the trend indicates that the variation in the critical stress intensity factors was directly related to the specific gravity. This trend is well defined indicating that the variation in specific gravities was a major factor which contributed to the scatter of critical stress intensity factors. However, no attempt was made to correct the experimental data because the scatter in Fig. 27 makes clear that any feasible method of measuring specific gravity would introduce an average value over a finite volume of wood. This would improve the appearance of the data but it also would introduce another variable, namely the volume of the strip used in specific gravity measurements. Since the specific gravity at the crack tip could not be measured, the data was used without an arbitrary correction. In its present form, the data showed the amount of scatter that must be expected in balsa wood. Had a more uniform orthotropic material been chosen for testing, scatter of the type shown in Fig. 24 undoubtedly would be reduced.

2. The accuracy of the crack measurements. The measurements are made through a single microscope. The location of one tip of the crack was first determined and the microscope was then moved to locate the other tip so that the crack length could be measured. This method was quite accurate when the crack was stable at low load levels. But as the fracture load was approached, the tip of the crack whose location was first determined did not necessarily remain stable while the microscope was moved to locate the other tip. Furthermore, in some cases, the tips of the crack were not well defined and precise measurement was difficult. However, since the "critical" crack length for each specimen was determined from the crack extension rate which was averaged from several crack measurements, the uncertainty of the crack measurements attributable to the two aforementioned difficulties was considerably reduced.

3. Constraint introduced by the side grips in the combined tension and shear tests. In the tests which followed path No. 3, side grips were required. The constraint of the side grips on the specimen was minimized as much as possible by the methods outlined in sections III A2 and III B, however it could not be eliminated during the crack extension process.

It can be seen that in the combined tension and shear tests which followed path No. 2 no side grips were required. The effect of the constraint of the grips on fracture strengths of the specimens can be examined by comparing the results of tests which follow path No. 3 to those which follow path No. 2. In Fig. 24, the data which are presented as open points were obtained from tests where side grips were used, and the data presented in solid points were obtained from tests where no side grips were present.

In the middle region, where both types of experiments were performed it can be seen that the data overlap about evenly. Thus it can be concluded that the constraint of the side grips was properly minimized, and its effect on fracture strength cannot be detected from the experimental results.

4. Buckling of the specimen under shear. Buckling occurred only when shear load was applied to the specimen with side grips in place. When buckling occurred, the fracture strength was greatly reduced, but when shear was induced by tests which followed path No. 2, no buckling was present. Once again, the data in Fig. 24 indicated that there was no significant difference between the data obtained by these two testing methods, and it can be concluded that buckling was successfully eliminated by the constraint system employed in the experiments* when shear load was applied through the side grips.

5. Absolute similitude was not maintained between the theoretical model in the analysis and the model used for experimental investigation. The imposed conditions** which were necessary for the mathematical analysis of the crack tip stress distribution will be compared one by one with the actual conditions of the experiments. First, the material was assumed to be linearly elastic. The specific gravity of the specimens varies from 0.126 to 0.220. The ultimate tensile strength and proportional limit perpendicular to the grain for balsa wood whose average specific gravity is .176 ranges from 118 to 170 psi and 100 to 144 psi respectively***. No data on the proportional limit for pure shear was available, however the range of shearing strengths is from 298 to 360 psi. In the experiments, the highest nominal stresses observed were 112 psi in tension and 258 psi in pure shear. Since the range of the strength properties is relatively large, it was not possible to examine the validity of the assumption of linear elasticity for every specimen, but it is clear that in a small region around the crack tips the stresses exceeded the limits of elastic behavior. Nevertheless, from the range of the values given above, it appeared that the nominal stress did not exceed the elastic limit with the exception of perhaps a few specimens containing very short cracks. In those cases, some plasticity correction was needed. However, since the data did not significantly deviate from a straight line of slope equal to $-1/2$ in the $\log \sigma$ vs $\log a$ and $\log \tau$ vs $\log a$ diagrams as predicted by the elastic analysis, no plasticity correction was attempted.

*

** This is described in section III A 2 and shown in Fig. 8.

*** These conditions are stated in section II A.

These properties are taken from the data published by the Balsa Ecuador Lumber Corporation, 500 Fifth Avenue, New York 36, New York. The proportional limits are obtained from compression tests.

Second, the plate was assumed to be thin and to extend to infinity in all directions from the crack. The ratio of the smallest dimension in the plane of the plate (the width $D = 4''$) to the thickness of the plate t was $\frac{D}{t} = 64$ which indicated that plane elasticity was applicable. Furthermore, the smallest ratio of the plate width W (at the line of the crack) to the crack length $2a$, was $\frac{W}{2a} = 3.6$. From experience with isotropic plates, it was known that edge effects of the plate on crack extension cannot be measured for $\frac{W}{2a} > 3$. It is therefore reasonable to conclude that the edge effect was negligible in these experiments.

Third, the crack was assumed to be straight and "sharp". A straight crack was cut into the specimen by a surgical knife blade approximately 0.02" thick. A knife blade whose width was smaller than the length of the crack was inserted in the center and flexed slightly to make the crack tip propagate a small distance. In this way a sharp natural crack was introduced in the specimen which corresponds closely to the theoretical assumption.

Fourth, the crack is assumed to be parallel to one of the principle planes of elastic symmetry. In the experimental program, only the case of the crack parallel to the grain of the wood was considered. It was very difficult to define the grain of the balsa wood precisely and consequently some error was introduced. But the variations in crack orientation were within $\pm 2^\circ$ from the average plane of elastic symmetry and no provision was made to account for errors thus introduced.

Fifth, the influence of environment is neglected. If the environmental conditions were constant for all of the experiments, its effects could have been neglected. However, due to the fact that there was no means of controlling the environment in the laboratory in which these experiments were carried out, the effects of temperature and humidity on fracture strength were not accounted for.

Although absolute similitude could not be obtained between the analytical and experimental model without unnecessarily complicating the experiments it is believed that the degree of similitude achieved was sufficient to warrant the conclusions.

IV. SUMMARY AND RECOMMENDATIONS FOR FURTHER INVESTIGATION

From the theoretical analysis of the stress in the vicinity of the tip of a crack in an orthotropic plate it was found that the stress distribution was dependent on the material constants and that stress singularity was of the order $r^{-1/2}$. Also the theoretical analysis indicated that stress intensity factors $k_1 = \sigma\sqrt{a}$ and $k_2 = \tau\sqrt{a}$ similar to those used for isotropic materials could be used as parameters to measure the strength of an orthotropic plate containing a crack. Furthermore, the existence of a functional relation between k_1 and k_2 was proposed.

In the experimental investigation on balsa wood plates, the stress intensity factor k_{1c} and k_{2c} were found to be constants for critical combinations of crack length and loads in the symmetrical and skew-symmetrical cases respectively. Moreover, the stress intensity factors were not only found to be applicable for combined symmetrical and skew-symmetrical loads, but they were related by the function:

$$\left(\frac{k_1}{k_{1c}}\right)^2 + \left(\frac{k_2}{k_{2c}}\right)^2 = 1. \quad (60)$$

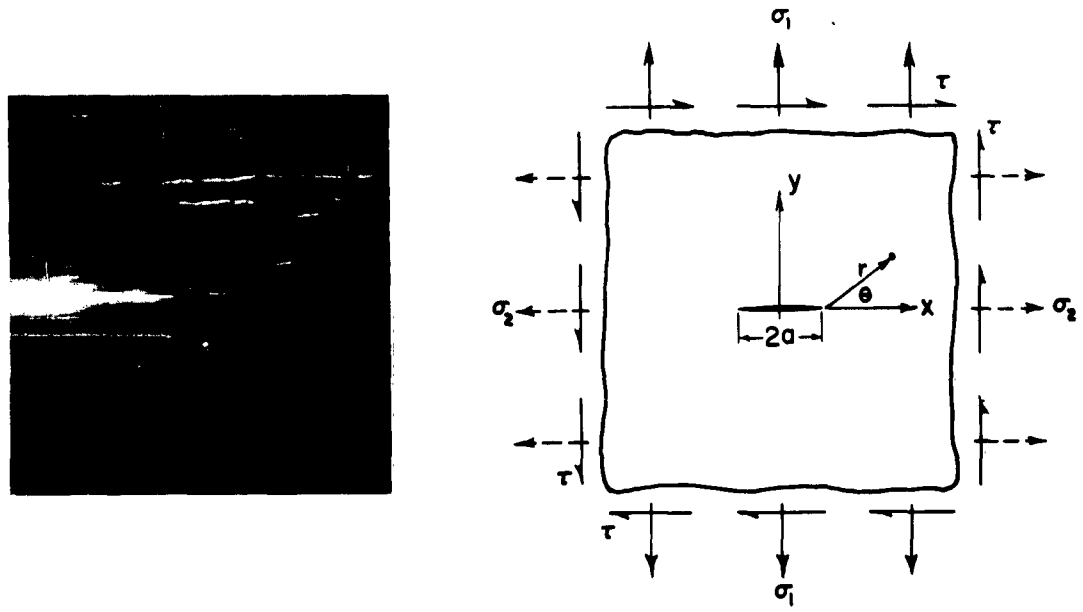
From the experimental results, a three dimensional representation of the relationship among the variables σ , τ and $2a$ is given in Fig. 28. In this figure, the surface relating σ , τ and $2a$ can be considered as a fracture surface. If the state of a cracked orthotropic plate is inside the tunnel shaped surface, unstable fracture is not probable but if the state is outside of this surface then fracture is likely. Thus, it can be seen that fracture mechanics can be applied to orthotropic materials.

Since the analysis deals with orthotropic plates of only one layer, the analysis should be extended to the more realistic case of multilayer orthotropic plates.

The experimental program was designed as a pilot test to see if fracture mechanics could be applied to orthotropic plates as suggested by the theoretical analysis and to explore any experimental problems. It was found that some refinements of the experimental set up were desirable. A tension-torsion filament wound tube specimen appears attractive for future work. Experimental investigation of multilayer specimens should be considered as a logical extension of this work in the future.

REFERENCES

1. Griffith, A. A. : "The Phenomenon of Rupture and Flow in Solids". Phil. Trans. Roy. Soc., London, Ser. A 221, 1920, pp. 163-196.
2. Irwin, G. G. : "Fracture", Handbuch der Physik, Vol. VI, Springer, 1958, pp. 551-590.
3. Milne-Thomson, L. M. : Plane Elastic Systems. Springer, 1960.
4. Savin, G. N. : Stress Concentration Around Holes. Pergamon Press, 1961.
5. Ang, D. D. and M. L. Williams: Combined Stresses in an Orthotropic Plate Having a Finite Crack, J. Appl. Mech. September, 1961, pp. 372-378.
6. Westergaard, H. M. : "Bearing Pressure and Crack," J. Appl. Mech. June 1939, pp. A-49 to A-53.
7. Irwin, G. R. : Analytical Aspects of Crack Stress Field Problems, University of Illinois T&AM Report No. 213, 1962.
8. Paris, P. E. : A Short Course in Fracture Mechanics. Lecture Notes, Presented at the Boeing Airplane Co., Transport Division, 1960.
9. Lekhnitskii, S. G. : Teoriya Uprugosti Anizotropnogo Tela, Moscow-Leningrad: Gostekhizdat, 1950.
10. Sih, G. S. and P. C. Paris: "The Stress Distribution and Stress Intensity Factors for a Crack Tip in an Anisotropic Plate Subjected to Extension". Lehigh University, Institute of Research, 1961.
11. Hearmon, R. F. S. : An Introduction to Applied Anisotropic Elasticity. Oxford University Press, 1961.
12. Chapkis, R. L. and M. L. Williams: "Stress Singularities for a Sharp-Notched Polarly Orthotropic Plate," Proc. of the 3rd U. S. Nat. Cong. of Appl. Mech., 1958, pp. 281-286.



(a) Crack Tip Shown at 10X (b) Plate Containing Single Crack Subjected to Symmetric and Skew-symmetric Traction

Fig. 1

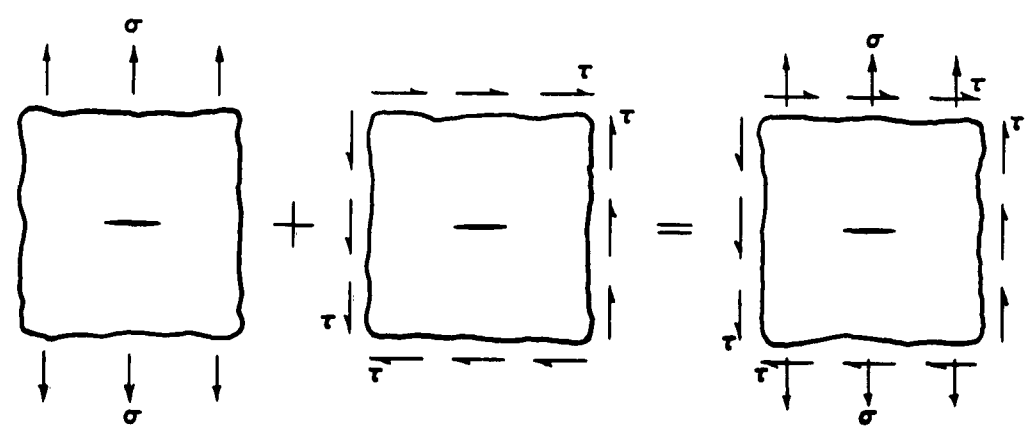
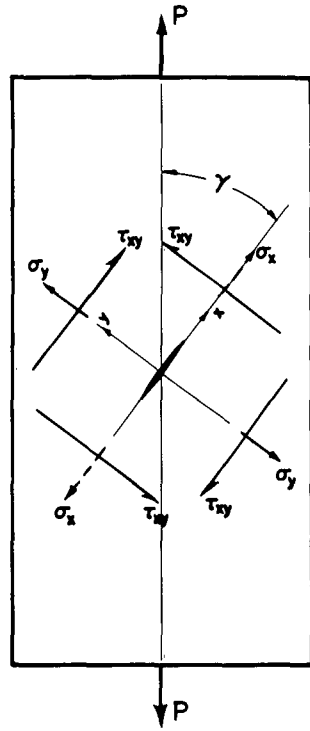


Fig. 2 Superposition of Symmetric Traction on Skew-symmetric Traction



$$\sigma_y = \sigma = P \sin^2 \gamma$$

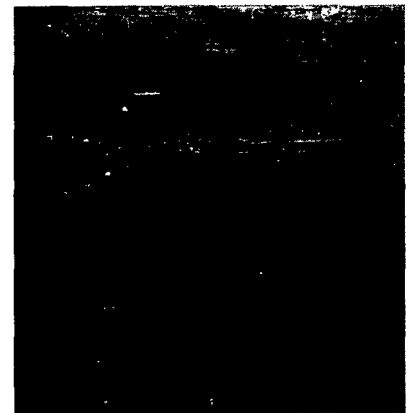
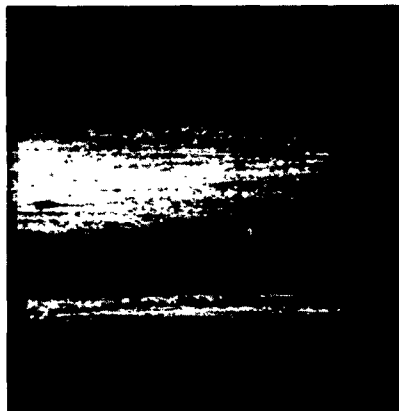
$$\tau_{xy} = \tau = P \sin \gamma \cos \gamma$$



(a) Components of Stress Around Crack Under Tension

(b) Typical Broken Tension Specimen

Fig. 3



(a) Photograph Illustrating Irregularities of Balsa Wood Specimen

(b) Typical Broken Shear Specimen

Fig. 4

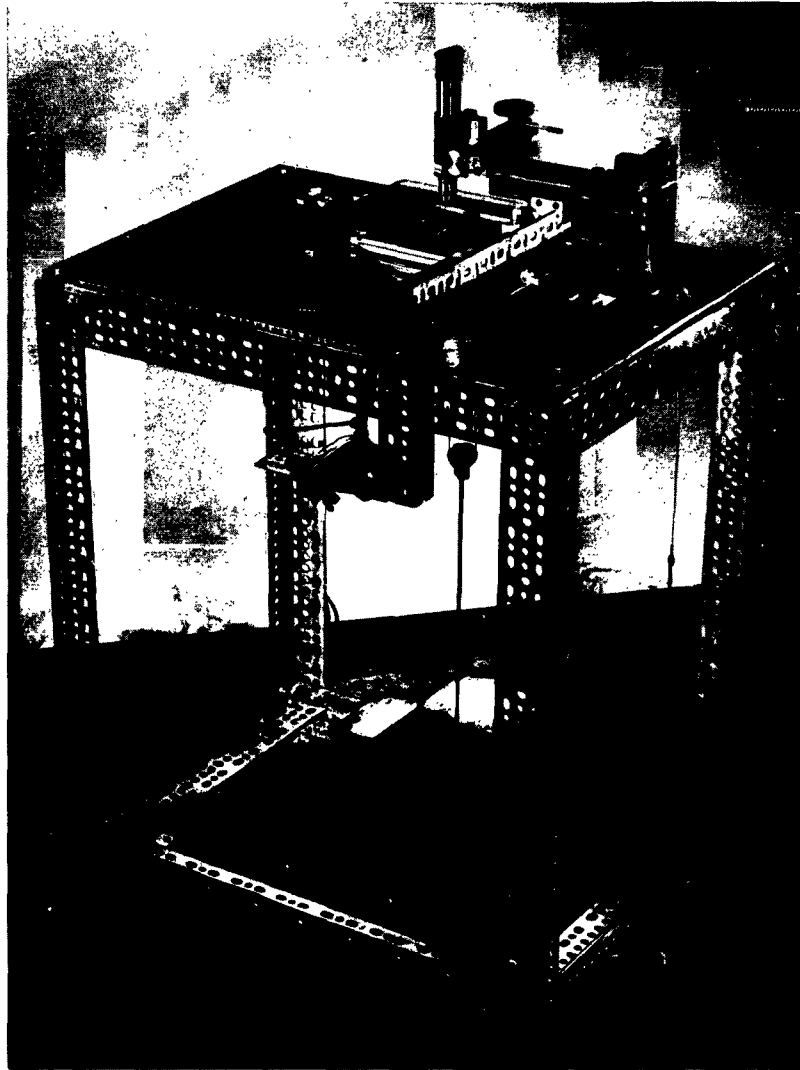
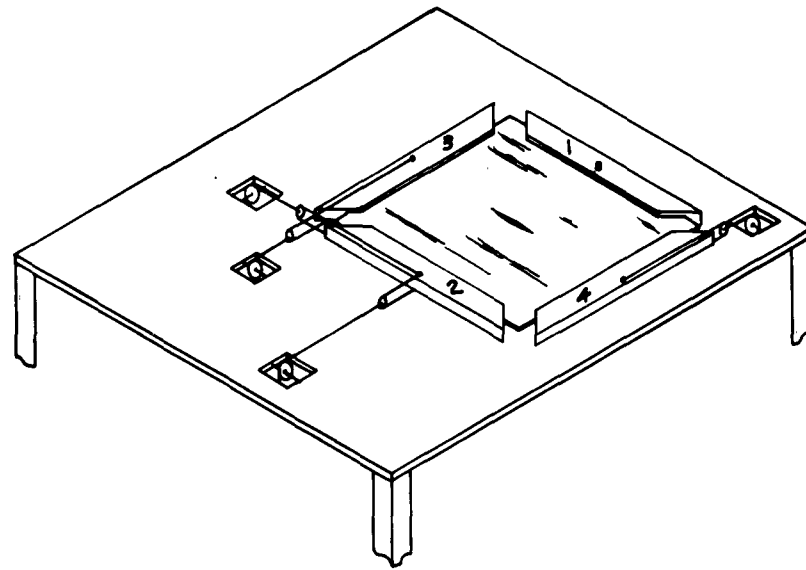
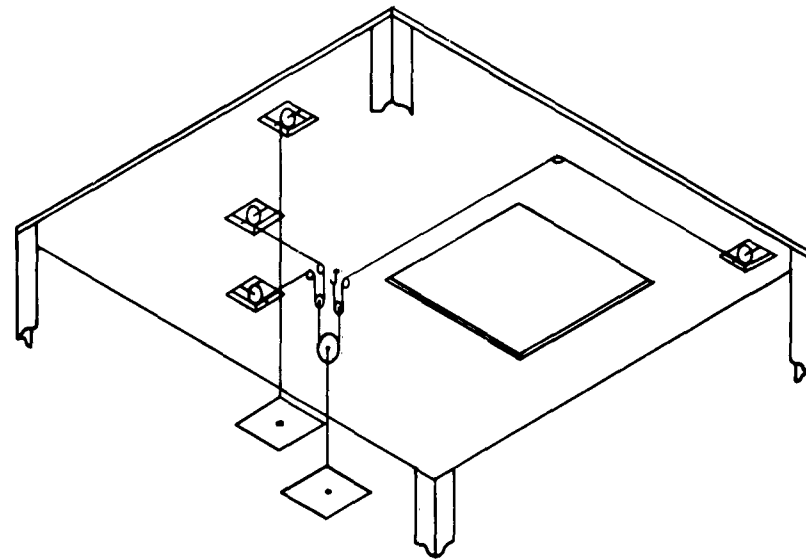


Fig. 5 Testing Machine



(a) Top View



(b) Bottom View

Fig. 6 Schematic Diagram of Essential Components of Testing Machine

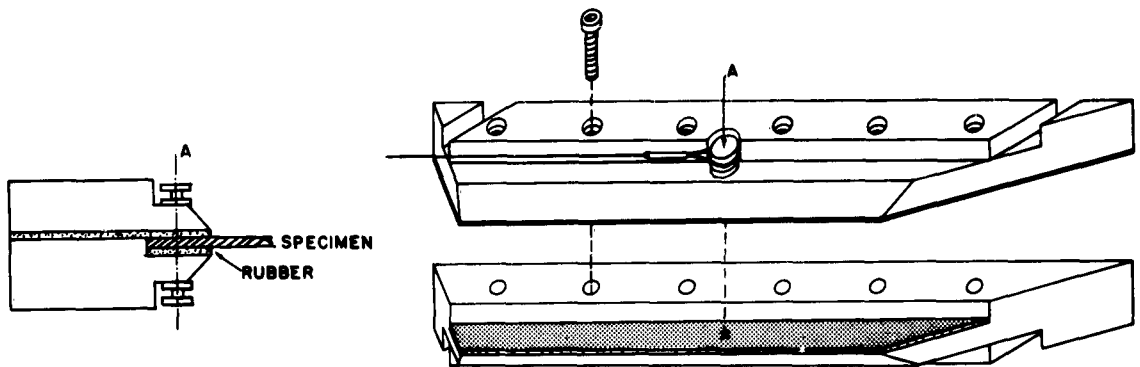


Fig. 7 Construction of Grips

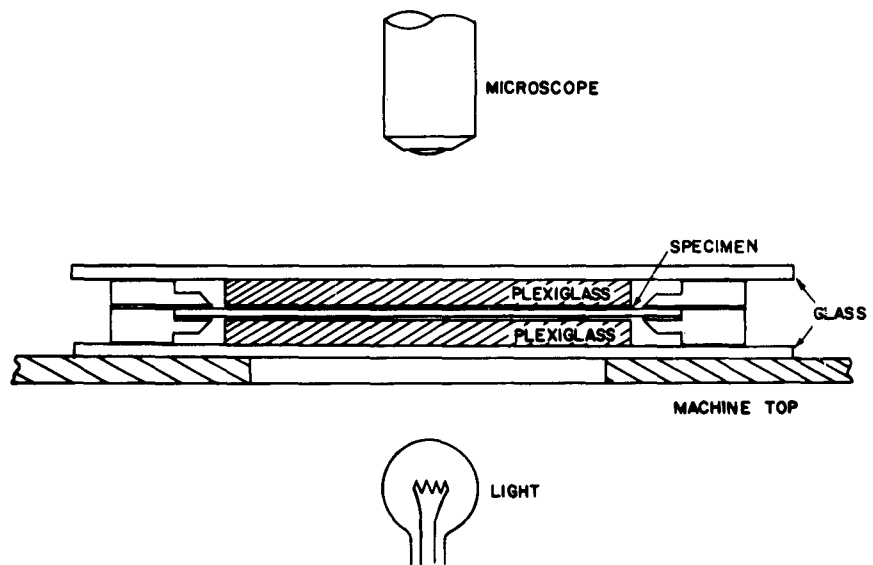


Fig. 8 Schematic Diagram of Cross Sectional View of Experimental Apparatus

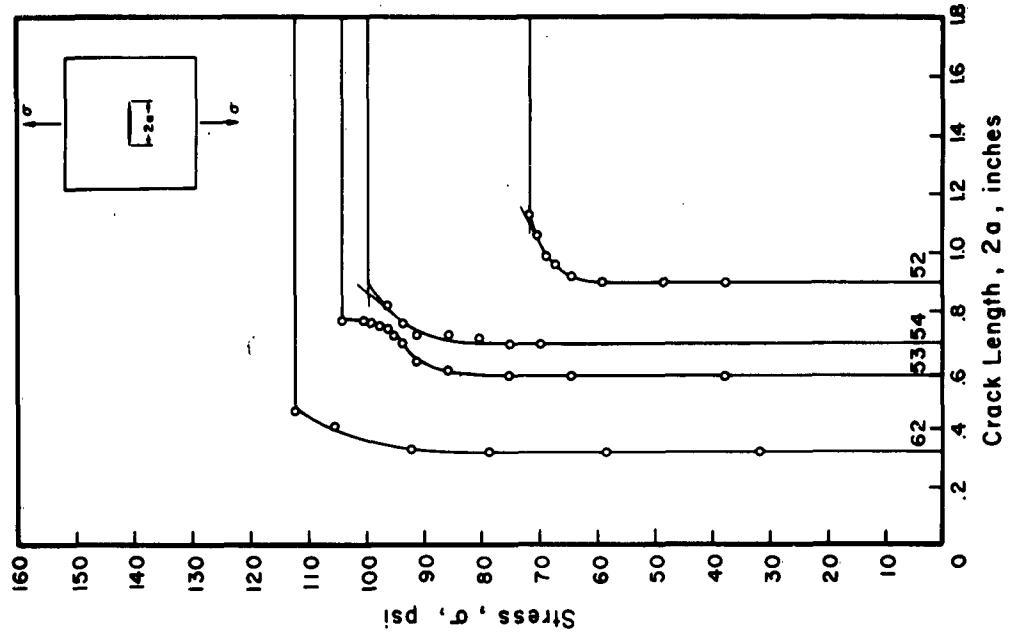


Fig. 10 Typical Crack Extension Patterns of Specimens Subjected to Tension, Path No. 1

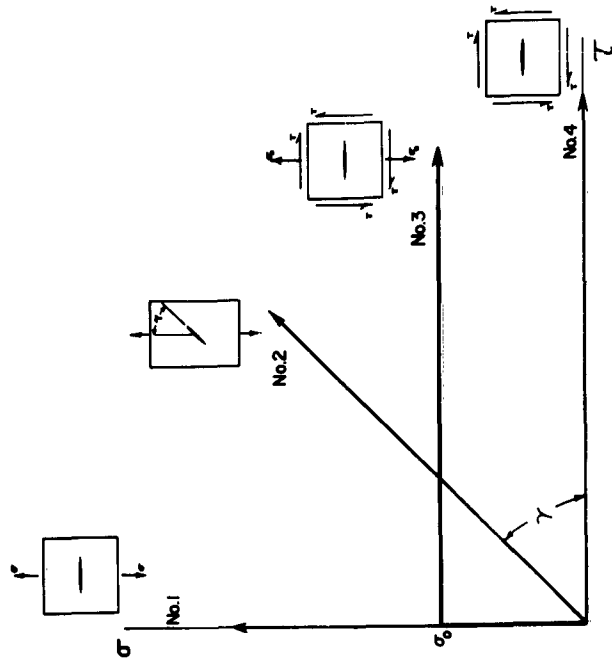
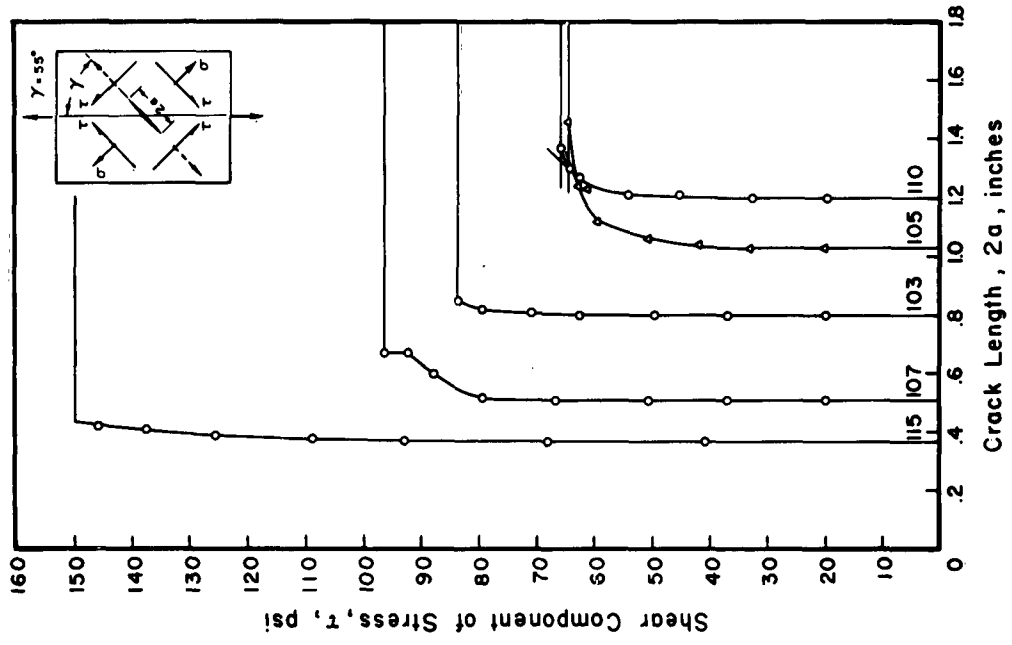
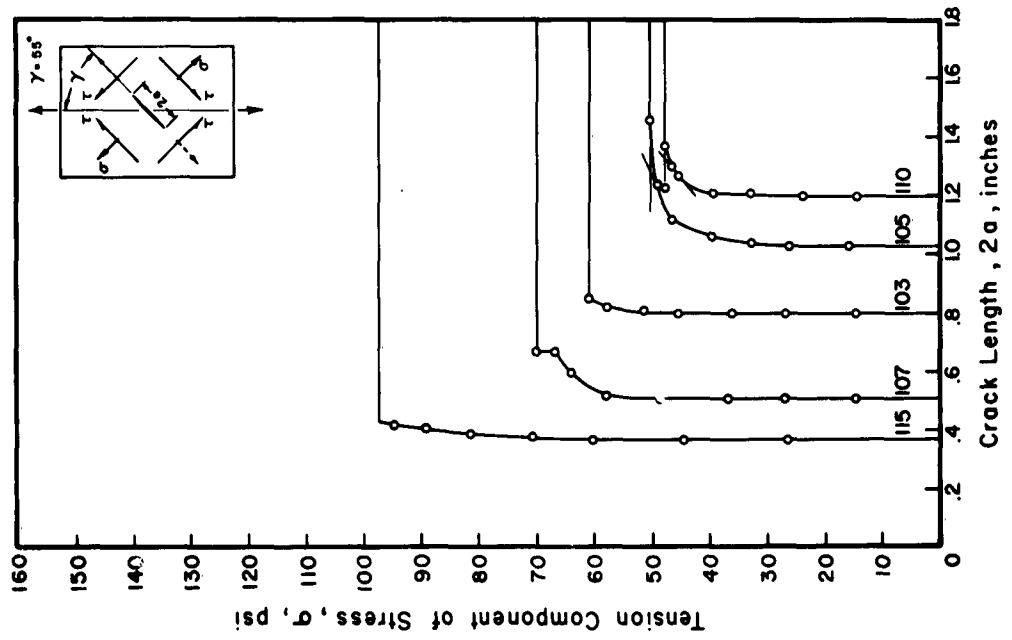


Fig. 9 Loading Paths Followed in Experiments



(a)



(b)

Fig. 11 Typical Crack Extension Patterns of Specimens Subjected to Tension, Path No. 2

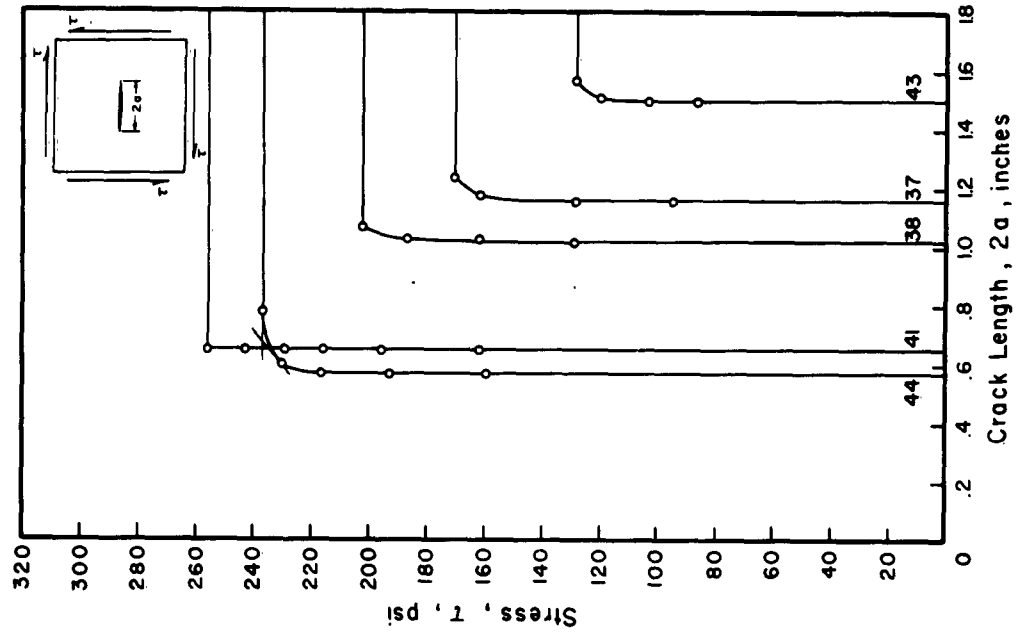


Fig. 13 Typical Crack Extension Patterns of Specimens Subjected to Pure Shear, Path No. 4

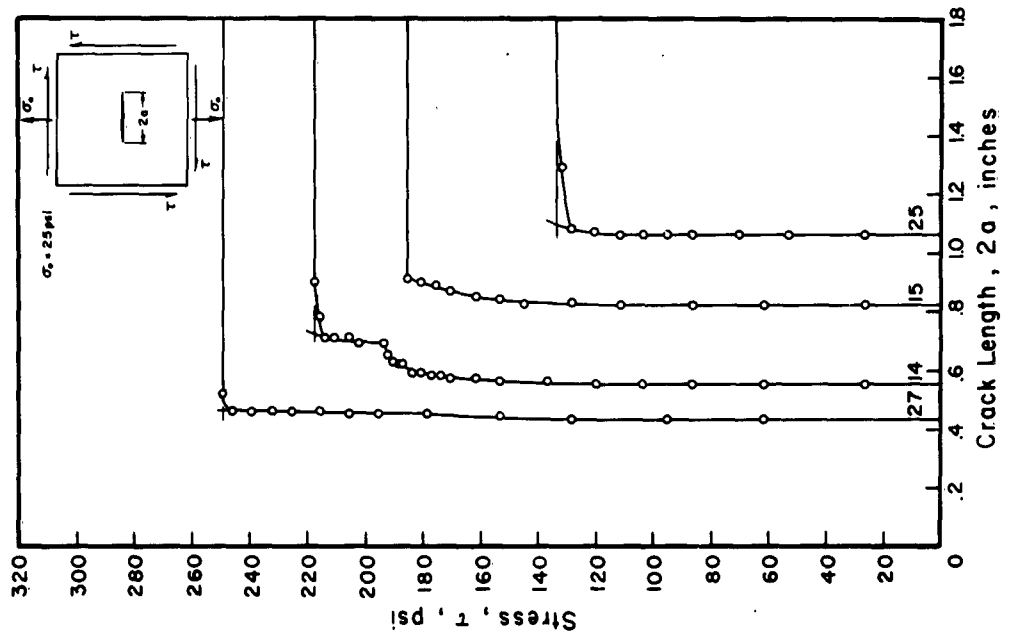


Fig. 12 Typical Crack Extension Patterns of Specimen Subjected to Combined Tension and Shear, Path No. 3

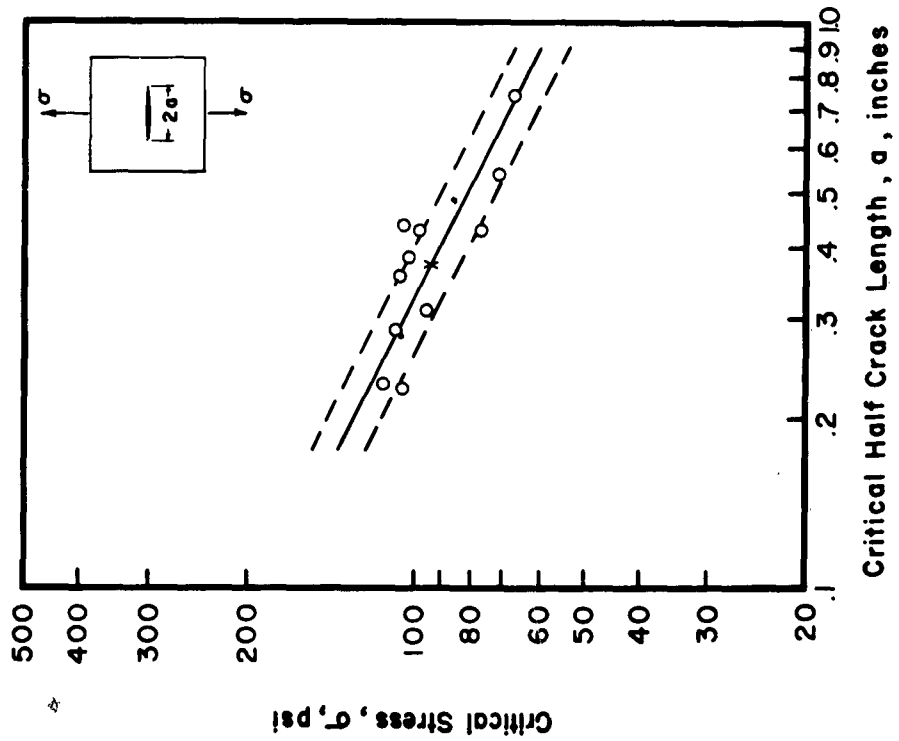


Fig. 14 Results of Tension Tests, Path No. 1

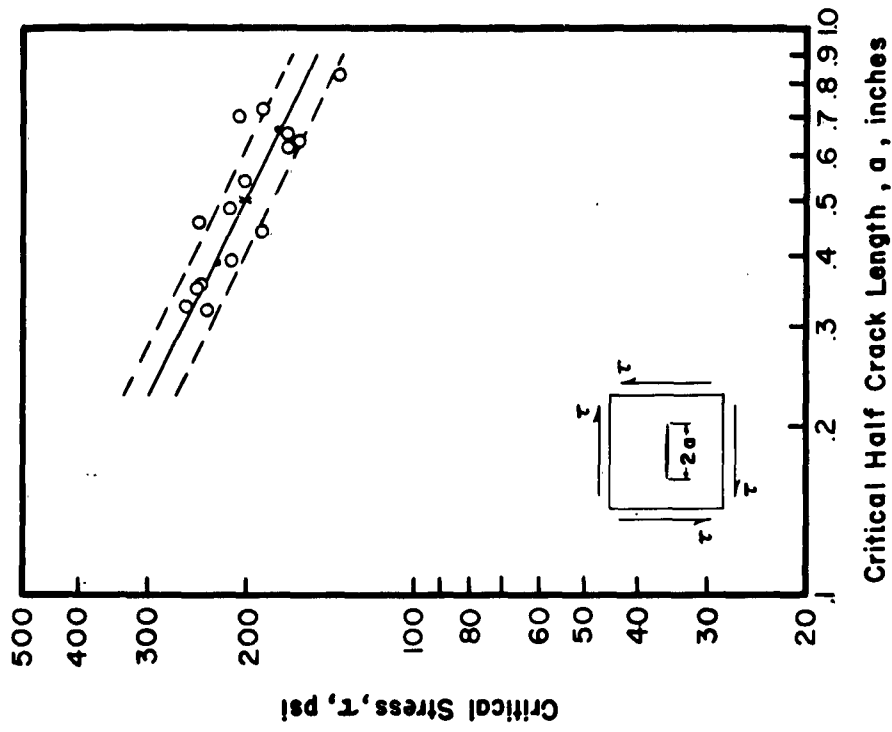


Fig. 15 Results of Shear Tests, Path No. 4

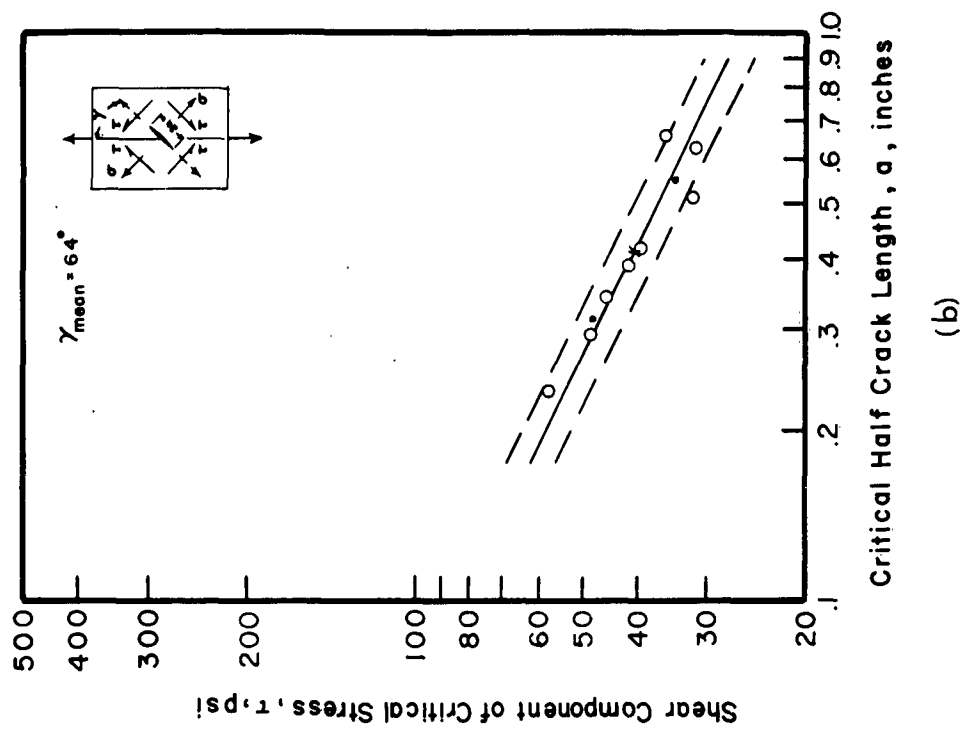
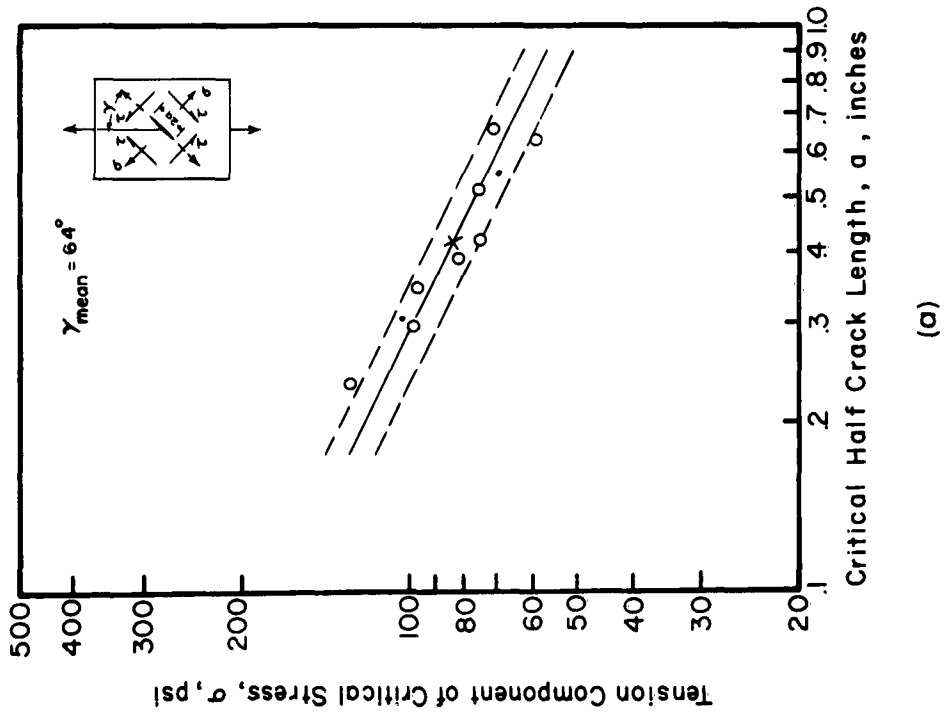
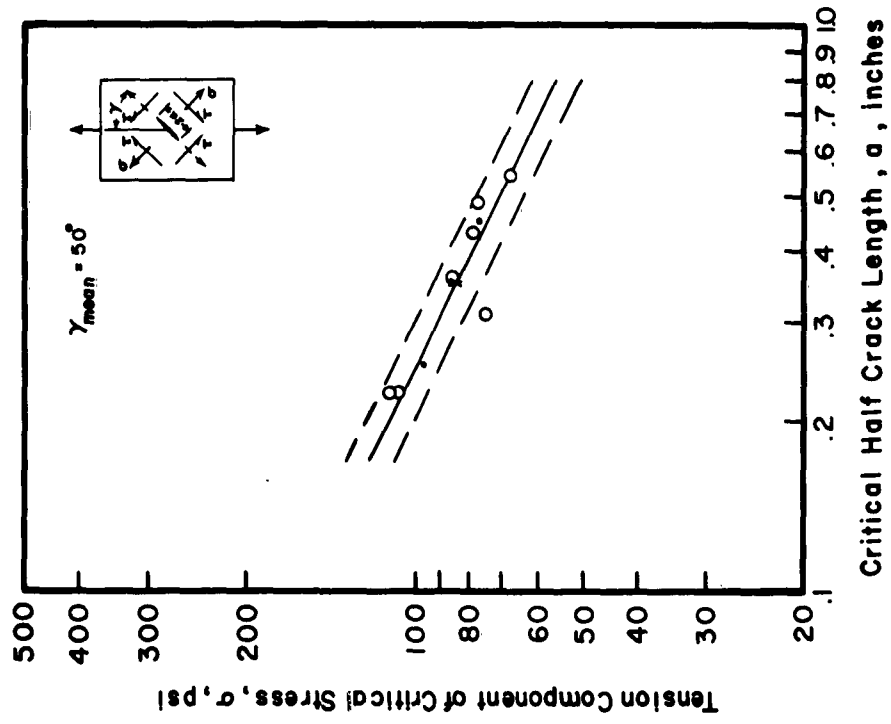
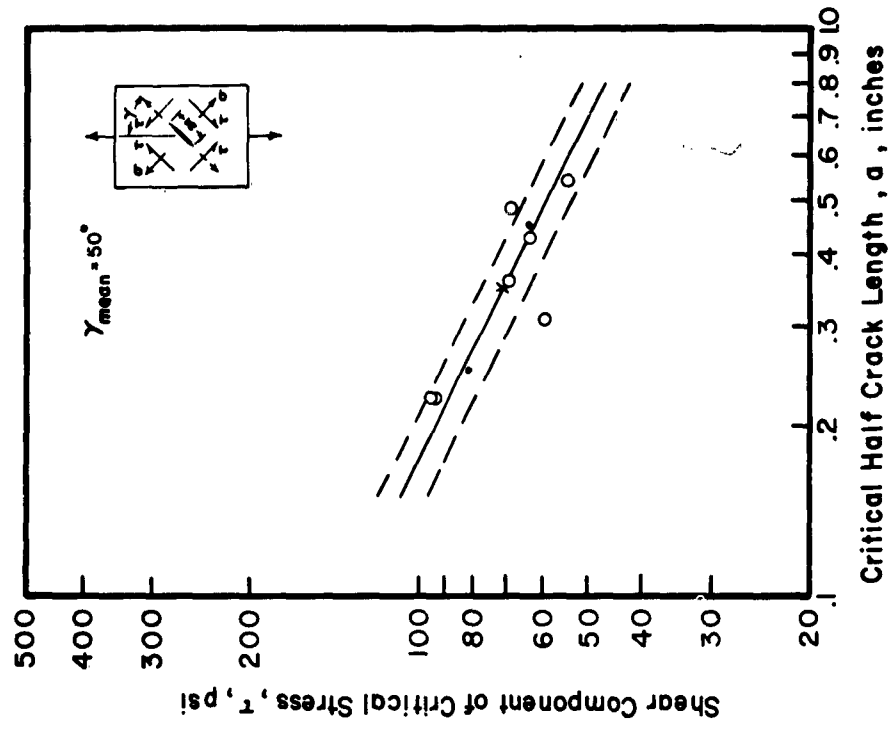


Fig. 16 Results of Tension Tests, Path No. 2 at $\gamma_{\text{mean}} = 64^\circ$



(a)



(b)

Fig. 17 Results of Tension Tests, Path No. 2 at $\gamma_{\text{mean}} = 50^\circ$

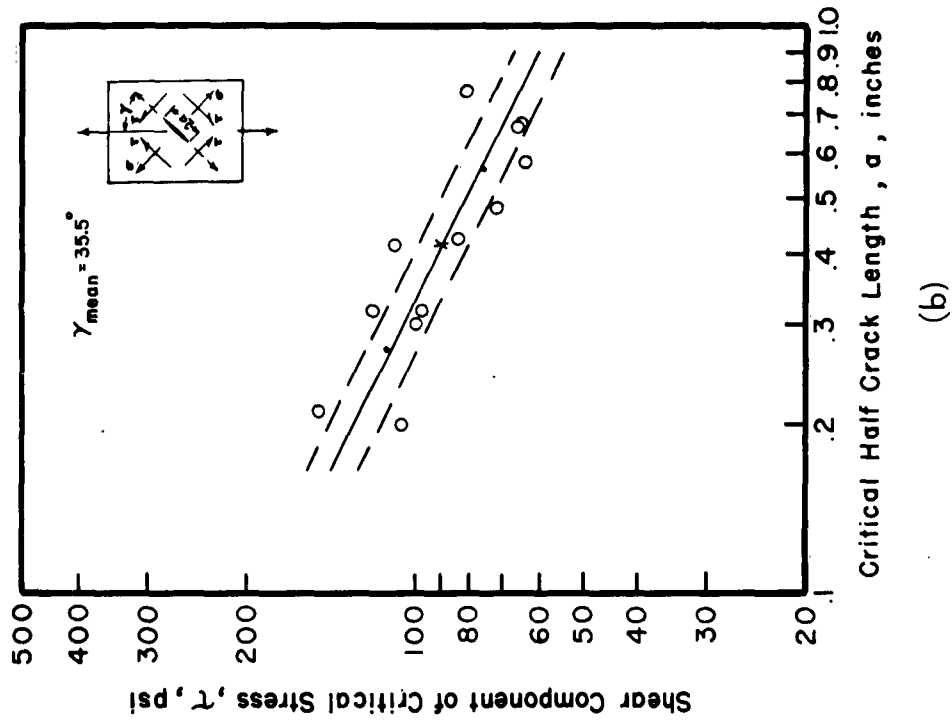
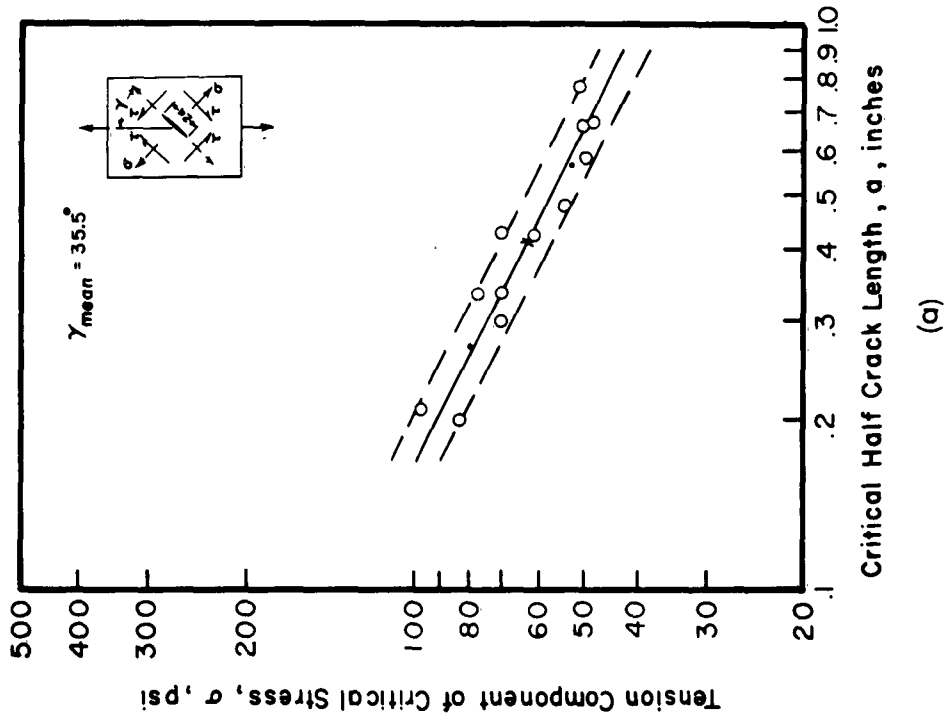
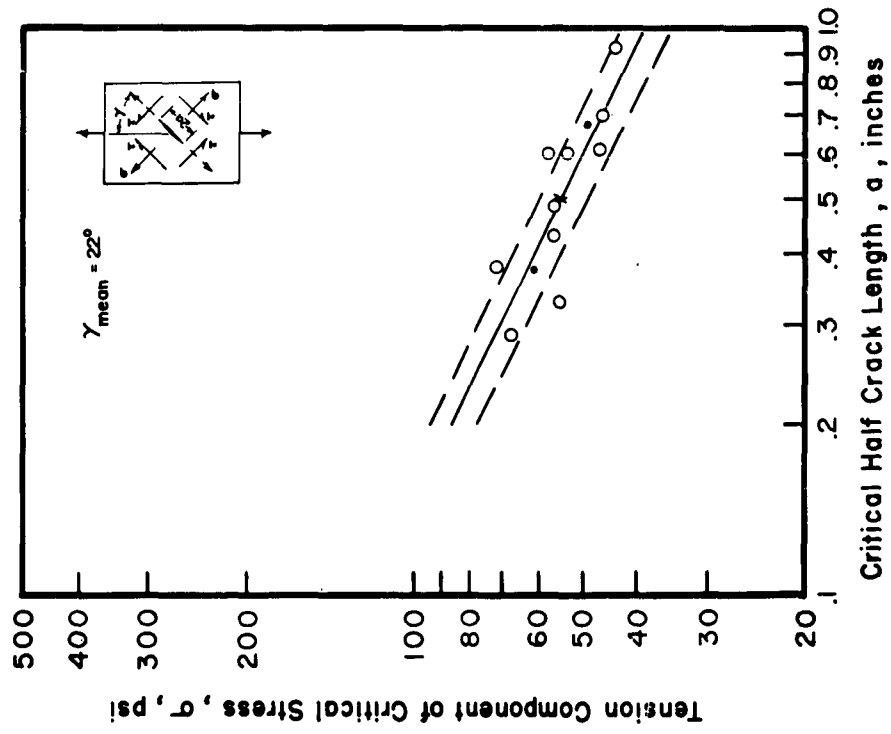
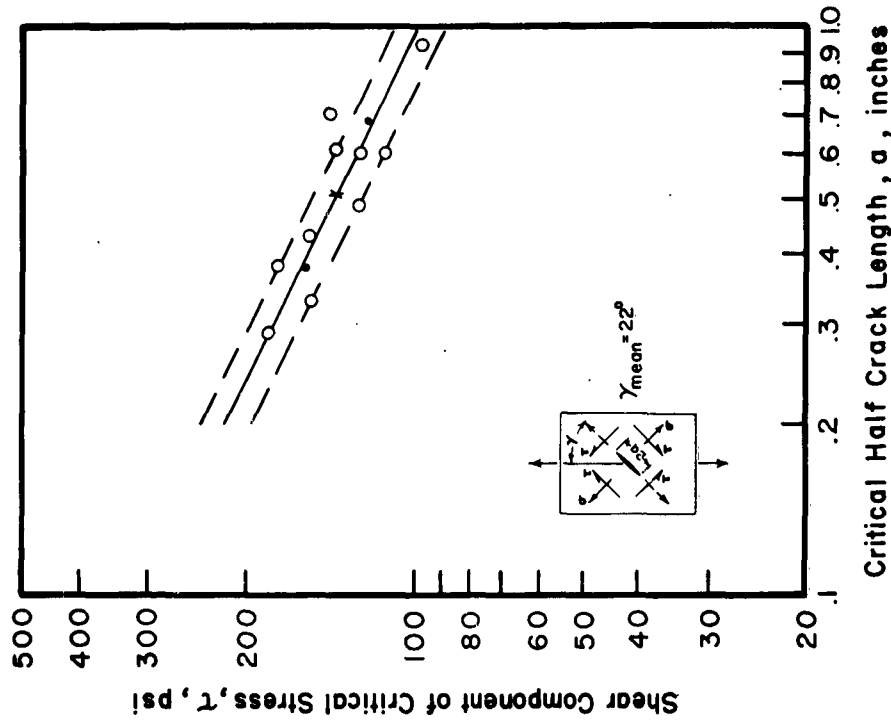


Fig. 18 Results of Tension Tests, Path No. 2 at $\gamma_{\text{mean}} = 35.5^\circ$



(a)



(b)

Fig. 19 Results of Tension Tests, Path No. 2 at $\gamma_{\text{mean}} = 22^\circ$

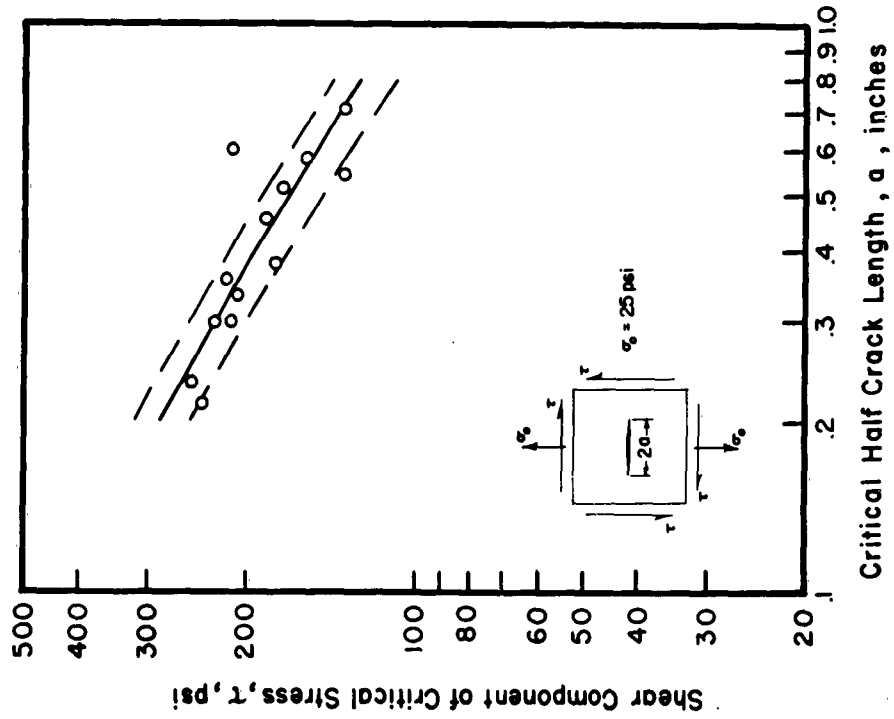


Fig. 20 Results of Combined Constant Tension and Shear Tests, Path No. 3, $\sigma_c = 25$ psi

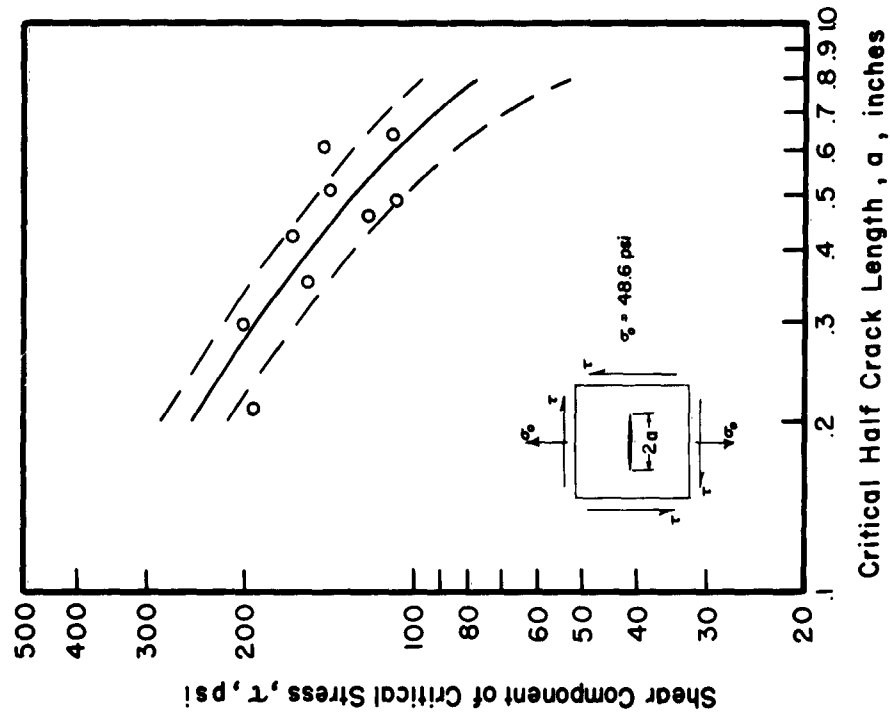


Fig. 21 Results of Combined Constant Tension and Shear Tests, Path No. 3, $\sigma_c = 48.6$ psi

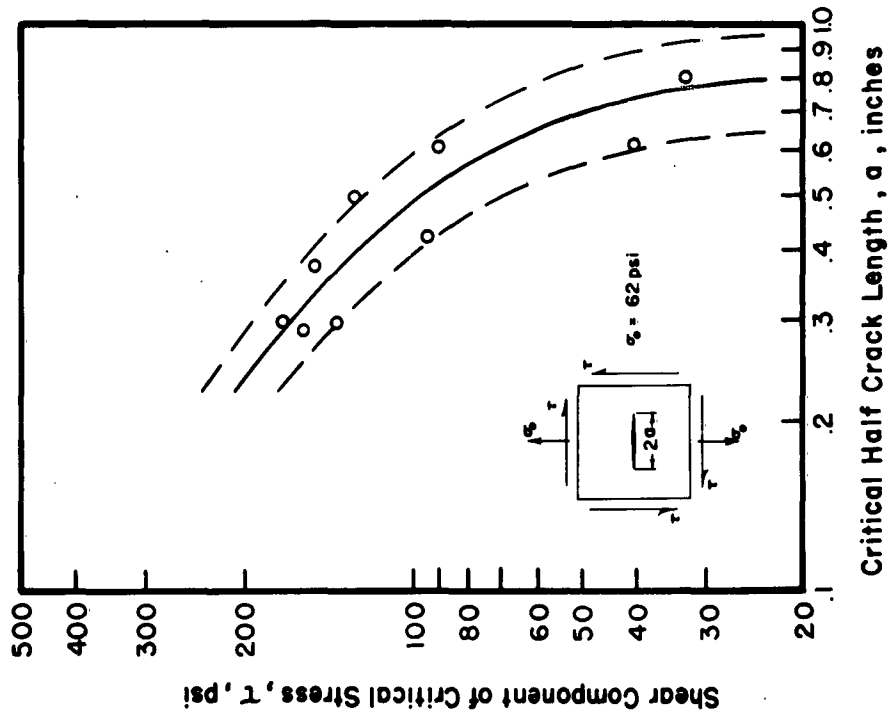


Fig. 22 Results of Combined Constant Tension and Shear Tests, Path No. 3, $\sigma_c = 62$ psi

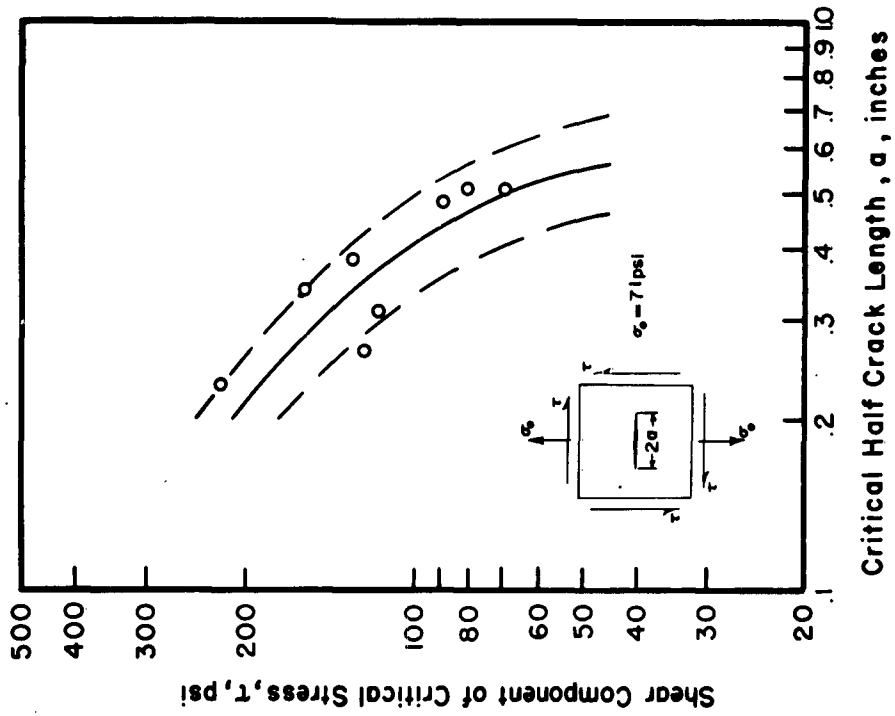


Fig. 23 Results of Combined Constant Tension and Shear Tests, Path No. 3, $\sigma_c = 71$ psi

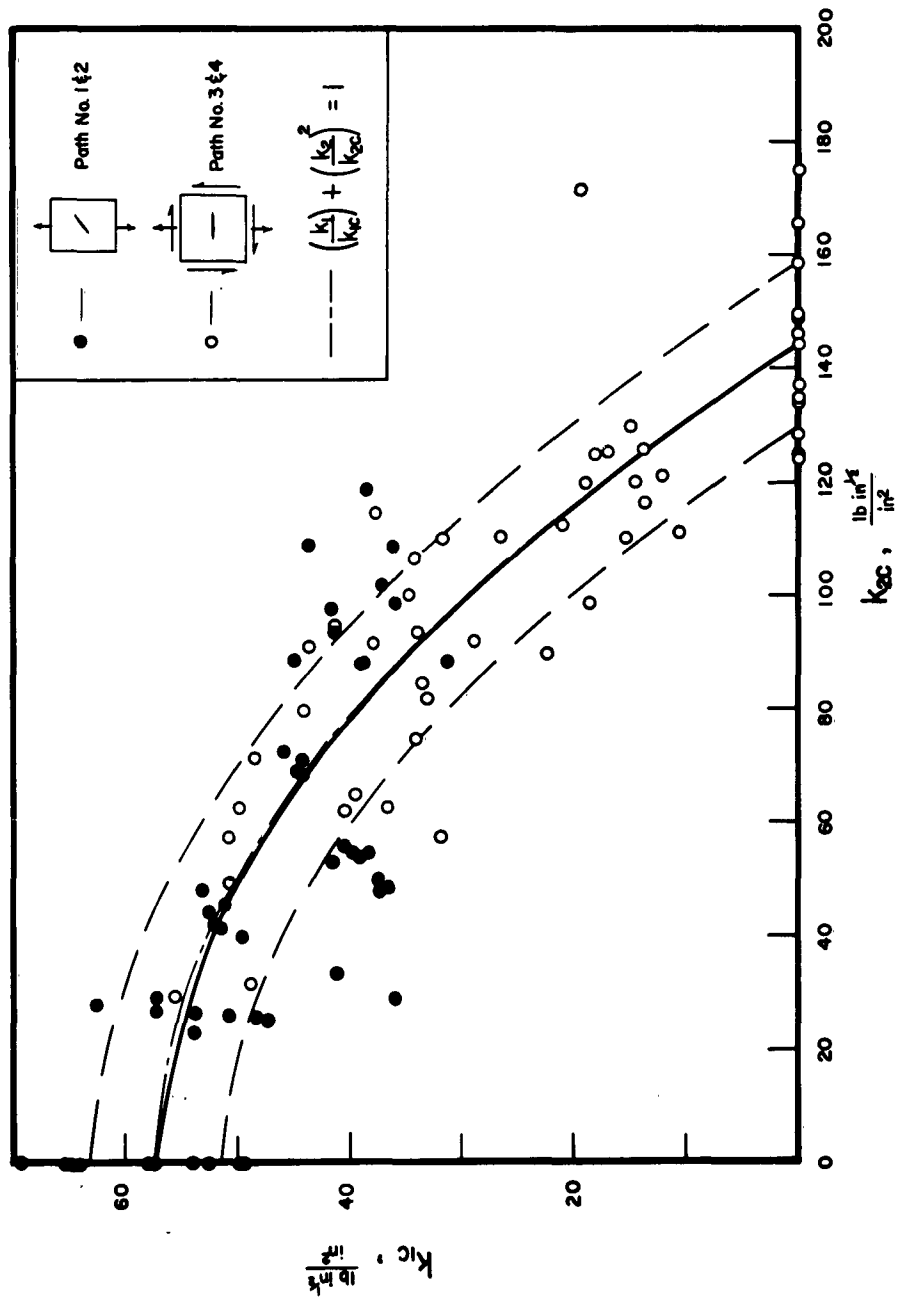


Fig. 24 Interaction Between Critical Symmetric Stress Intensity Factor K_{1c}
 and Critical Skew-symmetric Stress Intensity Factor k_{2c}

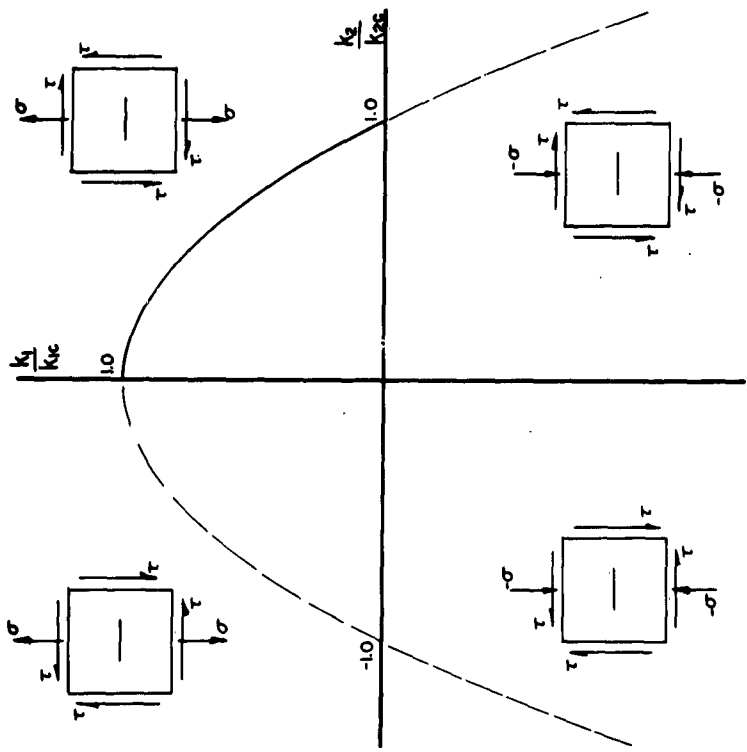


Fig. 26 Extension of Interaction Curve Between k_{1c} and k_{2c} to Compression

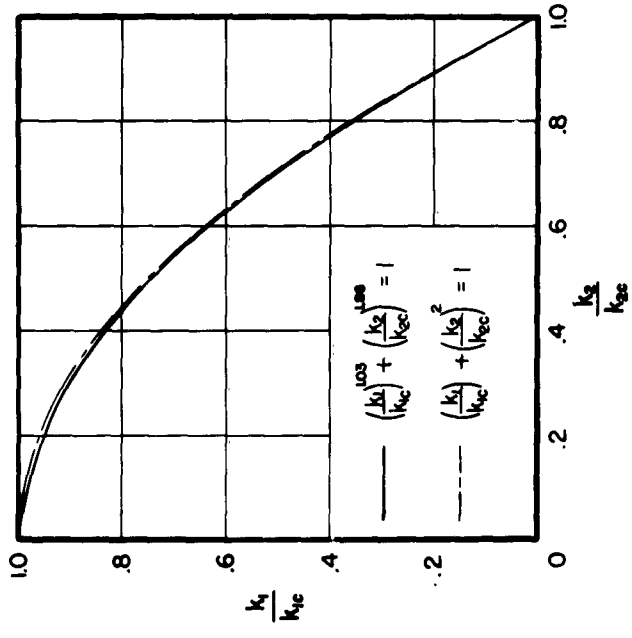


Fig. 25 Dimensionless Representation of Interaction Between Stress Intensity Factors k_{1c} and k_{2c}

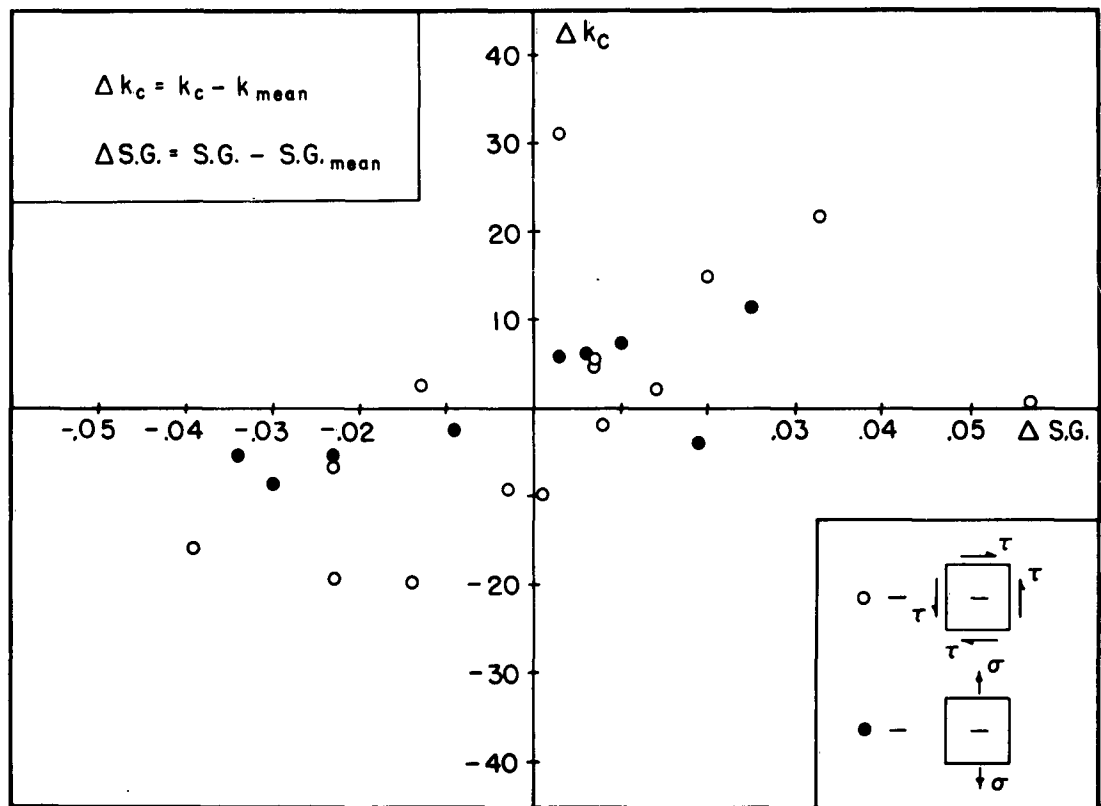


Fig. 27 Effect of Variation in Specific Gravity of Balsa Wood on Critical Stress Intensity Factors

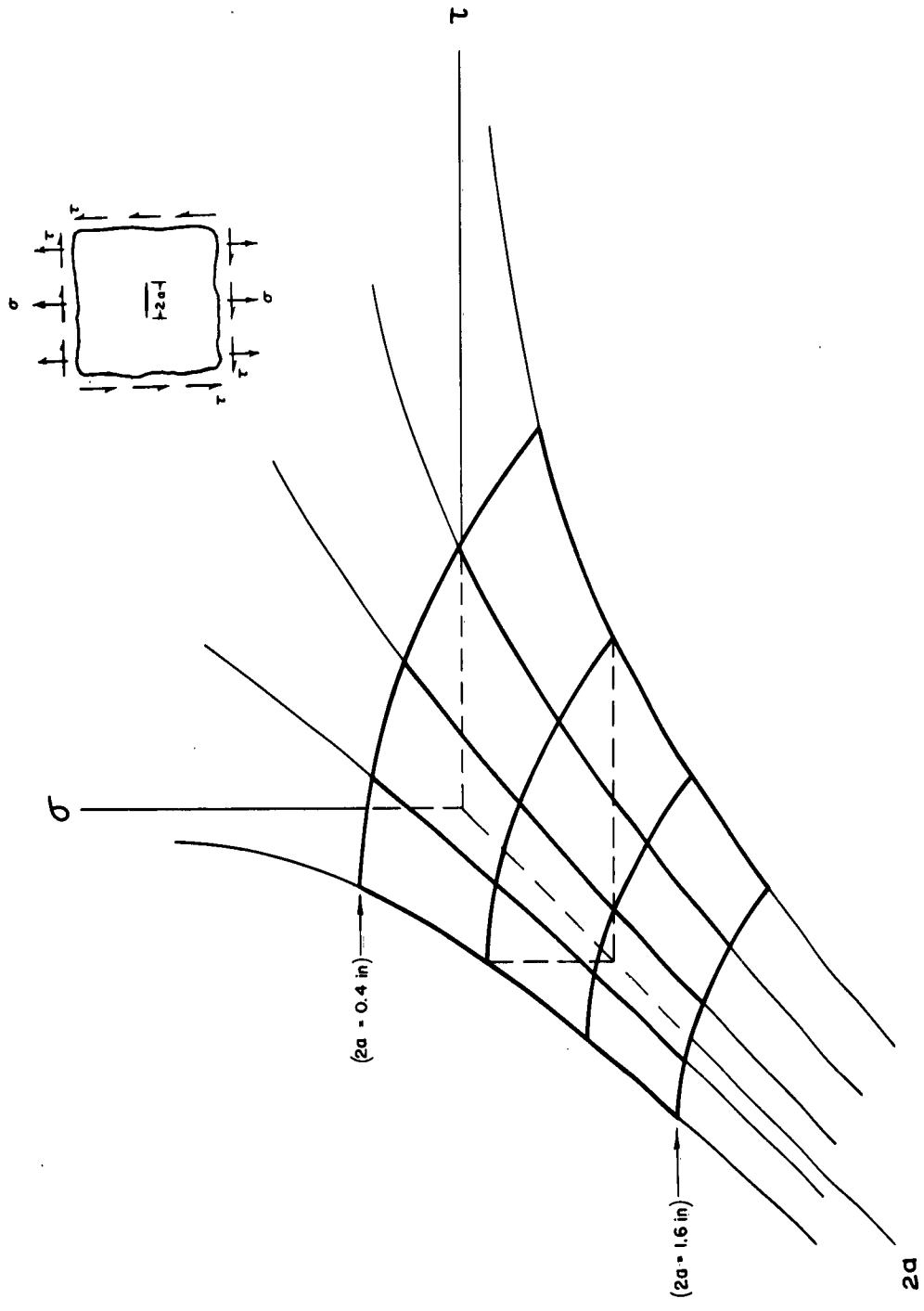


Fig. 28 3-Dimensional Representation of Experimentally Determined Fractured Surface

DISTRIBUTION LIST

for

FIBERGLASS DEVELOPMENT REPORTS

<u>Name</u>	<u>No. of copies</u>
U. S. Naval Research Laboratory Washington 25, D. C. Attn: Dr. P. King Code 6000	1
U. S. Naval Research Laboratory Washington 25, D. C. Attn: Dr. G. R. Irwin Code 6200	1
U. S. Naval Research Laboratory Washington 25, D. C. Attn: Mr. P. Waterman Code 5360	2
U. S. Naval Research Laboratory Washington 25, D. C. Attn: Mr. J. A. Kies Code 6210	10
U. S. Naval Research Laboratory Washington 25, D. C. Attn: Dr. Irwin Wolock Code 6213	1
U. S. Naval Research Laboratory Washington 25, D. C. Attn: Mrs. Doris Baster Code 2027	1
Department of the Navy Bureau of Naval Weapons Washington 25, D. C. Attn: Mr. H. Bernstein Code SP-2714	3
Department of the Navy Bureau of Naval Weapons Washington 25, D. C. Attn: Mr. Phillip M. Goodwin Code RRMA-3	1
Mr. W. Cohen, Code LPS National Aeronautics and Space Administration 1512 H Street, N. W. Washington 25, D. C.	1

<u>Name</u>	<u>No. of copies</u>
Bureau of Naval Weapons Resident Representative (Special Projects Office) c/o Hercules Powder Company Bacchus Works Magna, Utah	1
Narmco Industries, Inc. Research and Development Division 8125 Aero Drive San Diego, California Attn: Mr. W. Otto	1
Walter Kidde Company Aerospace Division Belleville, New Jersey Attn: Mr. T. Siuta	1
General Electric Company Schenectady, New York Attn: Mr. T. Jordan	1
Hercules Powder Company P. O. Box A Rocky Hill, New Jersey Attn: Mr. R. Carter	1
Rocketdyne Engineering A Division of North American Aviation, Inc. 6633 Canoga Avenue Canoga Park, California Attn : Mr. E. Hawkinson	1
Lockheed Missiles and Space Company A Division of Lockheed Aircraft Corp. 3251 Hanover Street Palo Alto, California Attn: Mr. M. Steinberg	1
Commander Aeronautical Systems Division ASRCNC-1 AF Systems Command U. S. Air Force Wright-Patterson AFB, Ohio	2
Plastic Evaluation Center Picatinny Arsenal Dover, New Jersey Attn: ORD-BB	1
Commander U. S. Naval Ordnance Test Station China Lake, California Attn: Mr. S. Herzog Code 5557	1

<u>Name</u>	<u>No. of copies</u>
Department of the Navy Bureau of Naval Weapons Washington 25, D. C. Attn: RMMP	2
Aerojet-General Corporation P. O. Box 296 Azusa, California Attn: Librarian	1
Jet Propulsion Laboratory 4800 Oak Grove Drive Pasadena 3, California Attn: I. E. Newlan Chief, Reports Group	1
Commander Armed Services Technical Information Agency Arlington Hall Station Arlington 12, Virginia	10
Department of the Army Office, Chief of Ordnance Washington 25, D. C.	1
Commander Army Rocket and Guided Missile Agency Redstone Arsenal, Alabama	1
Department of the Navy Bureau of Naval Weapons Washington 25, D. C. Attn: Technical Library	2
Allegany Ballistics Laboratory Hercules Powder Company Cumberland, Maryland Attn: Mr. R. Winer	2
Solid Propellant Information Agency Applied Physics Laboratory The Johns Hopkins University Silver Springs, Maryland Attn: G. McMurray	3
Hercules Powder Company Bacchus Works Magna, Utah Attn: Librarian	1

<u>Name</u>	<u>No. of copies</u>
Dr. N. LeBlanc Allegany Ballistics Laboratory Cumberland, Maryland	2
Mr. E. Rucks Aerojet-General Corporation Azusa, California	2
Dr. F. J. Climent Aerojet-General Corporation P.O. Box 1947 Sacramento, California	2
Mr. George Moe Lockheed Aircraft Corporation LMSD Headquarters Sunnyvale, California	2
Solar Aircraft Company San Diego Plant San Diego 12, California Attn: John V. Long	1
Professor John Outwater University of Vermont Burlington, Vermont	1
Professor H. T. Corten University of Illinois Urbana, Illinois	1
National Aeronautics and Space Administration 1512 H Street, N. W. Washington 25, D. C. Attn: Chief, Division of Research Information	1
Commander Air Force Ballistic Missile Division Hq. Air Res. and Devel. Command P. O. Box 262 Inglewood, California	1
Commanding General Aberdeen Proving Ground Maryland	1
Commanding Officer Picatinny Arsenal Dover, New Jersey	1
Commander Army Ballistic Missile Agency Redstone Arsenal, Alabama	1

<u>Name</u>	<u>No. of copies</u>
Lockheed Missiles and Space Company A Division of Lockheed Aircraft Corporation 1122 Jagels Road Sunnyvale, California Attn: Mr. H. H. Patton	1
Aerojet- General Corporation P. O. Box 1947 Sacramento, California Attn: Dr. W. O. Wetmore	5
Defense Metals Information Center Battelle Memorial Institute 505 King Avenue Columbus 1, Ohio	1
Commander U. S. Naval Ordnance Laboratory White Oak, Maryland	1
John I. Thompson and Company 1118 22nd Street, N. W. Washington 7, D. C.	1
The Bendix Corporation Bendix Products Division South Bend 20, Indiana Attn: Mr. Wade Hardy	1
Black, Sivalls and Bryson Oklahoma City, Oklahoma Attn: Mr. J. Carter	1
B. F. Goodrich Company 500 S. Main Akron, Ohio Attn: Mr. H. W. Stevenson	1
Goodyear Aircraft Corporation Akron 15, Ohio Attn: Mr. R. Burkley	1
Bureau of Naval Weapons Representative P.O. Box 504 Sunnyvale, California	1
Bureau of Naval Weapons Resident Representative P. O. Box 1947 Sacramento, California	1
Bureau of Naval Weapons Branch Representative Allegany Ballistics Laboratory Cumberland, Maryland Attn: Code 4	1

Name	<u>No. of copies</u>
Westinghouse Electric Corporation East Pittsburgh, Pennsylvania Attn: Mr. H. R. Sheppard	1
Professor H. H. Johnson Dept. of Engineering Mechanics and Materials Thurston Hall Cornell University Ithaca, New York	1
Mr. Don H. Bein, Director Research Economic Dept. A. O. Smith Corp. Milwaukee 1, Wisconsin	1
Mr. R. E. Jacobsen Aero-Space Division Boeing Airplane Company P.O. Box 3707 Seattle 24, Washington	

LIST OF RECENT REPORTS

<u>Number</u>	<u>Title and Author</u>	<u>Date</u>
230	"Final Report on Launcher Dynamics Study", by M. Stippes	October, 1962
231	"Cyclic Strain Accumulation Under Complex Multiaxial Loading", by G. J. Moyar and G. M. Sinclair	October, 1962
232	"Loads, Reactions, and Deflections for Sim- plified Artillery Pieces", by M. Stippes	October, 1962
233	"Final Report on Artillery Carriage Dynamic Study", by M. Stippes	October, 1962
234	"Miscroscopic Study of Mode of Fracture and Filament Wound Glass-Resin Composites", by C. A. Bouc	October, 1962
235	"Influence of Temperature and Strain Rate on Crack Toughness in Mild Steel", by A. K. Shoemaker	November, 1962
236	"Dislocation Arrangement in Aluminum De- formed by Repeated Tensile Stresses", by C. E. Feltner	November, 1962
237	"Response of a Linear Two Degree of Freedom System Excited by Two Distinct and Independent Frequencies", by J. A. Kasuba and W. J. Worley	November, 1962
238	"Plain and Deformed Wire Fabric in Concrete", by Russell S. Jensen, Albert C. Bianchini, and Clyde E. Kesler	February, 1963
239	"Cyclic-Dependent Stress-Strain Behavior of Metals", by F. R. Tuler and J. Morrow	March, 1963
240	"Relatively Unexplored Aspects of Fracture Mechanics", by G. A. Irwin	February, 1963
241	"An Application of Numerical Analysis for a Method of Conformal Mapping and the Deter- mination of Stresses in Solid-Propellant Rocket Grains", by Charles C. Fretwell	February, 1963
242	"The Phenomenon of Fracture and the Fracture Morphology of Glass Tested in Tension, Flexure and Torsion, by N. M. Cameron.	April, 1963
243	"A Method of Conformal Mapping and the Deter- mination of Stresses in Solid-Propellant Rocket Grains", by Howard B. Wilson, Jr.	April, 1963